
Towards a Better Global Loss Landscape of GANs

Ruoyu Sun, Tiantian Fang, Alex Schwing
University of Illinois at Urbana-Champaign
ruoyus, tf6, aschwing@illinois.edu

Abstract

Understanding of GAN training is still very limited. One major challenge is its non-convex-non-concave min-max objective, which may lead to sub-optimal local minima. In this work, we perform a global landscape analysis of the empirical loss of GANs. We prove that a class of separable-GAN, including the original JS-GAN, has exponentially many bad basins which are perceived as mode-collapse. We also study the relativistic pairing GAN (RpGAN) loss which couples the generated samples and the true samples. We prove that RpGAN has no bad basins. Experiments on synthetic data show that the predicted bad basin can indeed appear in training. We also perform experiments to support our theory that RpGAN has a better landscape than separable-GAN. For instance, we empirically show that RpGAN performs better than separable-GAN with relatively narrow neural nets. The code is available at <https://github.com/AilsaF/RS-GAN>.

1 Introduction

Generative Adversarial Nets (GANs) [35] are a successful method for learning data distributions. Current theoretical efforts to advance understanding of GANs often focus on statistics or optimization.

On the statistics side, Goodfellow et al. [35] built a link between the min-max formulation and the J-S (Jenson-Shannon) distance. Arjovsky and Bottou [3] and Arjovsky et al. [4] proposed an alternative loss function based on the Wasserstein distance. Arora et al. [5] studied the generalization error and showed that both the Wasserstein distance and J-S distance are not generalizable (i.e., both require an exponential number of samples). Nevertheless, Arora et al. [5] argue that the real metric used in practice differs from the two statistical distances, and can be generalizable with a proper discriminator. Bai et al. [7] and Lin et al. [58] analyzed the potential “lack of diversity”: two different distributions can have the same loss, which may cause mode collapse. Bai et al. [7] argue that proper balancing of generator and discriminator permits both generalization and diversity.

On the optimization side, cyclic behavior (non-convergence) is well recognized [65, 8, 34, 11]. This is a generic issue for min-max optimization: a first-order algorithm may cycle around a stable point, converge very slowly or even diverge. The convergence issue can be alleviated by more advanced optimization algorithms such as optimism (Daskalakis et al. [23]), averaging (Yazıcı et al. [88]) and extrapolation (Gidel et al. [33]).

Besides convergence, another general optimization challenge is to avoid sub-optimal local minima. It is an important issue in non-convex optimization (e.g., Zhang et al. [91], Sun [81]), and has received great attention in matrix factorization [31, 14, 19] and supervised learning [38, 47, 2, 92, 27]. For GANs, the aforementioned works [65, 8, 34, 11] either analyze convex-concave games or perform local analysis. Hence they do not touch the global optimization issue of non-convex problems. Mescheder et al. [65] and Feizi et al. [30] prove global convergence only for simple settings where the true data distribution is a single point or a single Gaussian distribution. The global analysis of GANs for a fairly general data distribution is still a rarely touched direction.

The global analysis of GANs is an interesting direction for the following reasons. **First**, from a theoretical perspective, it is an indispensable piece for a complete theory. To put our work in

Table 1: Comparison of theoretical works.

	Supervised Learning		GANs	
	paper	brief description	paper	brief description
Generalization analysis	[9]	generalization bound for neural-nets	[5]	generalization bound for GANs
Convergence analysis	[77]	convex problem, divergence of Adam convergence of AMSGrad	[23]	bi-linear game, non-convergence of GDA convergence of optimistic GDA
Global landscape	[73] [50]	Any distinct input data Wide neural-nets have no sub-optimal basins	This work	Any distinct input data SepGAN has bad basins; RpGAN does not

* This table does NOT show a complete list of works. The goal is to list various types of works. Only one or two works are listed as examples of that class.

perspective, we compare representative works in supervised learning with works on GANs in Tab. 1. **Second**, it may help to understand mode collapse. Bai et al. [7] conjectured that a lack of diversity may be caused by optimization issues, albeit convergence analysis works [65, 8, 34, 11] do not link non-convergence to mode collapse. Thus we suspect that mode collapse is at least partially related to sub-optimal local minima, but a formal theory is still lacking. **Third**, it may help to understand the training process of GANs. Even understanding a simple two-cluster experiment is challenging because the loss values of min-max optimization are fluctuating during training. Global analysis can provide an additional lens in demystifying the training process.

Additional related work is reviewed in Appendix A.

Challenges and our solutions. While the idea of a global analysis is natural, there are a few obstacles. First, it is hard to follow a common path of supervised learning [38, 47, 2, 92, 27] to prove global convergence of gradient descent for GANs, because the dynamics of non-convex-non-concave games are much more complicated. Therefore, we resort to a *landscape analysis*. Note that our approach resembles an “equilibrium analysis” in game theory. Second, it was not clear which formulation can cure the landscape issue of JS-GAN. Wasserstein GAN (W-GAN) is a candidate, but its landscape is hard to analyze due to the extra constraints. After analyzing the issue of JS-GAN, we realize that the idea of “paring”, which is implicitly used by W-GAN, is enough to cure the issue. This leads us to consider relativistic pairing GANs (RpGANs) [41, 42] that couple the true data and generated data¹. We prove that RpGANs have a better landscape than separable-GANs (generalization of JS-GAN). Third, it was not clear whether the theoretical finding affects practical training. We make a few conjectures based on our landscape theory and design experiments to verify those. Interestingly, the experiments match the conjectures quite well.

Our contributions. This work provides a global landscape analysis of the empirical version of GANs. Our contributions are summarized as follows:

- *Does the original JS-GAN have a good landscape, provably?* For JS-GAN [35], we prove that the outer-minimization problem has exponentially many sub-optimal strict local minima. Each strict local minimum corresponds to a mode-collapse situation. We also extend this result to a class of separable-GANs, covering hinge loss and least squares loss.
- *Is there a way to improve the landscape, provably?* We study a class of relativistic pairing GANs (RpGANs) [41] that pair the true data and the generated data in the loss function. We prove that the outer-minimization problem of RpGAN has no bad strict local minima, improving upon separable-GANs.
- *Does the improved landscape lead to any empirical benefit?* Based on our theory, we predict that RpGANs are more robust to data, network width and initialization than their separable counter-parts, and our experiments support our prediction. Although the empirical benefit of RpGANs was observed before [41], the aspects we demonstrate are closely related to our landscape theory. In addition, using synthetic experiments we explain why mode-collapse (as bad basins) can slow down JS-GAN training.

2 Difference of Population Loss and Empirical Loss

Goodfellow et al. [35] proved that the population loss of GANs is convex in the space of probability densities. We highlight that this convexity highly depends on a simple property of the population loss, which may vanish in an empirical setting.

Suppose p_{data} is the data distribution, p_g is a generated distribution and $D \in C_{(0,1)}(\mathbb{R}^d)$, where $C_{(0,1)}(\mathbb{R}^d)$ is the set of continuous functions with domain \mathbb{R}^d and codomain $(0, 1)$. Consider the

¹In fact, we proposed this loss in a first version of this paper, but later found that [41, 42] considered the same loss. We adopt their name RpGAN from [42].

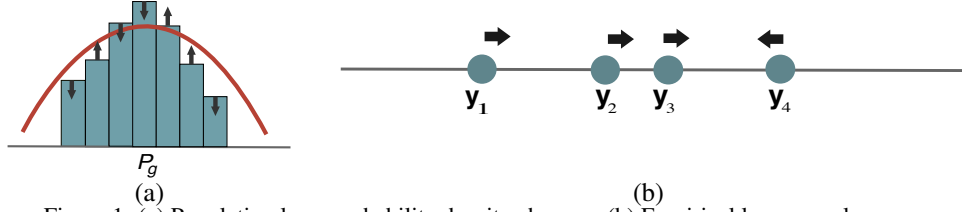


Figure 1: (a) Population loss: probability density changes; (b) Empirical loss: samples move.

JS-GAN formulation [35]

$$\min_{p_g} \phi_{\text{JS}}(p_g; p_{\text{data}}), \text{ where } \phi_{\text{JS}}(p_g; p_{\text{data}}) = \sup_D \mathbb{E}_{x \sim p_{\text{data}}, y \sim p_g} [\log(D(x)) + \log(1 - D(y))].$$

Claim 2.1. ([35, in proof of Prop. 2]) *The objective function $\phi_{\text{JS}}(p_g; p_{\text{data}})$ is convex in p_g .*

The proof utilizes two facts: first, the supremum of (infinitely many) convex functions is convex; second, $\mathbb{E}_{x \sim p_{\text{data}}, y \sim p_g} [\log(D(x)) + \log(1 - D(y))]$ is a linear function of p_g . The second fact is the essence of the argument, which we restate below in a more general form.

Claim 2.2. $\mathbb{E}_{y \sim p_g} [f^{\text{arb}}(y)]$ is a linear function of p_g , where $f^{\text{arb}}(y)$ is an arbitrary function of y .

Claim 2.2 implies that $\min_{p_g} \mathbb{E}_{y \sim p_g} [f^{\text{arb}}(y)]$ is a convex problem. One approach to solve it is to draw finitely many samples (particles) $y_i, i = 1, \dots, n$ from p_g , and approximate the population loss by the empirical loss. See Fig. 1 for a comparison of the probability space and the particle space. For an arbitrarily complicated function such as $f^{\text{arb}}(y) = \sin(\|y\|^8 + 2\|y\|^3 + \log(\|y\|^4 + 1))$, the population loss is convex in p_g , but clearly the empirical loss is non-convex in (y_1, \dots, y_n) . This example indicates that studying the empirical loss may better reveal the difficulty of the problem (especially with a limited number of samples). See Appendix G for more discussions.

We focus on the empirical loss in this work. Suppose there are n data points x_1, \dots, x_n . We sample n latent variables $z_1, \dots, z_n \in \mathbb{R}^{d_z}$ according to a rule (e.g., i.i.d. Gaussian) and generate artificial data $y_i = G(z_i), i = 1, \dots, n$. The empirical version of JS-GAN addresses $\min_Y \phi_{\text{JS}}(Y, X)$ where

$$\phi_{\text{JS}}(Y, X) \triangleq \sup_D \frac{1}{2n} \sum_{i=1}^n [\log(D(x_i)) + \log(1 - D(y_i))]. \quad (1)$$

Note that the empirical loss is considered in Arora et al. [5] as well, but they study the generalization properties. We focus on the optimization properties, which is complementary to their work.

3 Landscape Analysis of GANs: Intuition and Toy Results

In this section, we discuss the main intuition and present results for a 2-point distribution.

Intuition of Bad “Local Minima” and Separable-GAN:

Consider an empirical data distribution consisting of two samples $x_1, x_2 \in \mathbb{R}$. The generator produces two data points y_1, y_2 to match x_1, x_2 . We illustrate the training process of JS-GAN in Fig. 2. Initially, y_1, y_2 are far from x_1, x_2 , thus the discriminator can easily separate true data and fake data. After the generator update, y_1, y_2 cross the decision boundary to fool the discriminator. Then, after the discriminator update, the decision boundary moves and can again separate true data and fake data. As iterations progress, y_1, y_2 and the decision boundary may stay close to x_1 , causing mode-collapse.

The intuition above is the starting point of this work. We notice that Unterthiner et al. [83], Li and Malik [53] presented somewhat similar intuition, and Kodali et al. [45] suggested the connection between mode collapse and a bad equilibrium. Nevertheless, Li and Malik [53], Kodali et al. [45] do not present a theoretical result, and Unterthiner et al. [83] uses a significantly different formulation from standard GANs. See Appendix A for more.

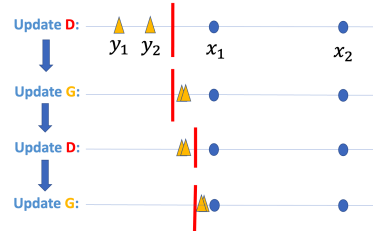


Figure 2: Issue of separable-GAN (including JS-GAN). After updating G , fake data crosses boundary to fool D ; after updating D , they are separated by D . Fake data may be stuck near x_1 .

We point out that a major reason for the above issue is a single decision boundary which judges the generated samples. Therefore, this issue exists not only for the JS-GAN, but also for a large class of GANs which we call separable-GANs:

$$\min_Y \sup_f \sum_{i=1}^n h_1(f(x_i)) + h_2(-f(y_i)), \quad (2)$$

where h_1, h_2 are fixed scalar functions, such as $h_1(t) = h_2(t) = -\log(1 + e^{-t})$ and $h_1(t) = h_2(t) = -\max\{0, 1 - t\}$, and f is chosen from a function space (e.g., a set of neural-net functions).

Pairing as Solution: Rp-GAN. A natural solution is to use a different “decision boundary” for every generated point, e.g., pairing x_i and y_i , as illustrated in Fig. 3.

A suitable loss is the relativistic pairing GAN (RpGAN)²

$$\min_Y \sup_f \sum_{i=1}^n h(f(x_i) - f(y_i)), \quad (3)$$

where h is a fixed scalar function and f is chosen from a function space. RS-GAN (relative standard GAN) is a special case where $h(t) = -\log(1 + e^{-t})$. More specifically, RS-GAN addresses $\min_Y \phi_{\text{RS}}(Y, X)$ where

$$\phi_{\text{RS}}(Y, X) \triangleq \sup_f \frac{1}{n} \sum_{i=1}^n \log \frac{1}{1 + \exp(f(y_i) - f(x_i))}. \quad (4)$$

W-GAN [3] can be viewed as a variant of RpGAN where $h(t) = t$, with extra Lipschitz constraint.

We wonder how the issue of separable-GANs relates to “local minima” and how “pairing” helps. We present results for JS-GAN and RS-GAN for the two-point case below.

Global Landscape of 2-Point Case: Depending on the positions of y_1, y_2 , there are four states s_0, s_{1a}, s_{1b}, s_2 . They represent the four cases $|\{x_1, x_2\} \cap \{y_1, y_2\}| = 0$, $y_1 = y_2 \in \{x_1, x_2\}$, $|\{x_1, x_2\} \cap \{y_1, y_2\}| = 1$, and $\{x_1, x_2\} = \{y_1, y_2\}$ respectively. Training often starts from the “no-recovery” state s_0 , and ideally should end at the “perfect-recovery” state s_2 . There are two intermediate states: s_{1a} means all generated points fall into one mode (“mode collapse”); s_{1b} means one generated point is the true data point while the other is not a desired data point, which we call “mode dropping”³. The first three states can transit to each other (assuming continuous change of Y), but only s_{1b} can transit to s_2 . We illustrate the landscape of $\phi_{\text{JS}}(Y; X)$ and $\phi_{\text{RS}}(Y; X)$ in Fig. 4, by indicating the values in different states. The detailed computation is given next.

JS-GAN 2-Point Case: The range of $\phi_{\text{JS}}(Y, X)$ is $[-\log 2, 0]$. The value for the four states are:

Claim 3.1. *The minimal value of $\phi_{\text{JS}}(Y, X)$ is $-\log 2$, achieved at $\{y_1, y_2\} = \{x_1, x_2\}$.*

$$\phi_{\text{JS}}(Y, X) = \begin{cases} -\log 2 \approx -0.6931 & \text{if } \{x_1, x_2\} = \{y_1, y_2\}, \\ -\log 2/2 \approx -0.3467 & \text{if } |\{x_1, x_2\} \cap \{y_1, y_2\}| = 1, \\ \frac{1}{4}(2 \log 2 - 3 \log 3) \approx -0.4774 & \text{if } y_1 = y_2 \in \{x_1, x_2\}, \\ 0 & \text{if } |\{x_1, x_2\} \cap \{y_1, y_2\}| = \emptyset. \end{cases}$$

We illustrate the landscape of $\phi_{\text{JS}}(Y, X)$ in Fig. 4(a). As a corollary of the above claim, the outer optimization of the original GAN has a bad strict local minimum at state s_{1a} (a mode-collapse).

Corollary 3.1. $\bar{Y} = (x_1, x_1)$ is a sub-optimal strict local-min of the function $g(Y) = \phi_{\text{JS}}(Y, X)$.

RS-GAN 2-Point Case: The range is still $\phi_{\text{RS}}(Y, X) \in [-\log 2, 0]$. The values are:

Claim 3.2. *The minimal value of $\phi_{\text{RS}}(Y, X)$ is $-\log 2$, achieved at $\{y_1, y_2\} = \{x_1, x_2\}$. In addition,*

$$\phi_{\text{RS}}(Y, X) = \begin{cases} -\log 2 \approx -0.6931 & \text{if } \{x_1, x_2\} = \{y_1, y_2\}, \\ -\frac{1}{2} \log 2 \approx -0.3466 & \text{if } |\{i : \exists j, \text{ s.t. } x_i = y_j\}| = 1, \\ 0 & \text{otherwise.} \end{cases}$$

²Our motivation of considering RpGAN because it breaks locality, thus possibly admitting a better landscape. This motivation is somewhat different from Jolicoeur-Martineau [41, 42].

³Both may be called mode collapse. Here we differentiate “mode collapse” and “mode dropping”.

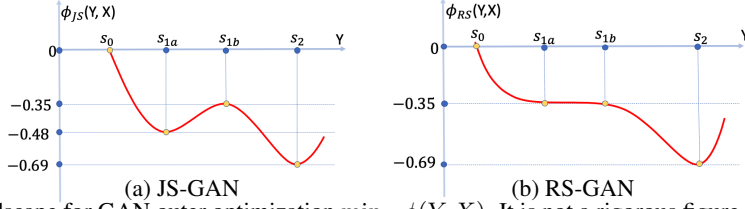


Figure 4: Landscape for GAN outer optimization $\min_Y \phi(Y, X)$. It is not a rigorous figure because: (i) there are only four possible values, thus the function is piece-wise linear while we use smooth curves for accessibility. (ii) the landscape should be two-dimensional, but we illustrate them in 1D space. Nevertheless, it is still useful for understanding GAN training, as discussed later in Section 5 and Appendix B.

We illustrate $\phi_{RS}(Y, X)$ in Fig. 4(b). Importantly, note that the only basin is the global minimum. In contrast, the landscape of JS-GAN contains a bad basin at a mode-collapsed pattern.

The proofs of Claim 3.1 and Claim 3.2 are given in Appendix H. We briefly explain the main insight provided by these proofs. For the mode-collapsed pattern s_{1a} , the loss value of JS-GAN is $-\frac{1}{4} \min_{s,t} [\log(1 + e^{-t}) + 2 \log(1 + e^t) + \log(1 + e^{-s})] = \frac{1}{4} (\log \frac{1}{3} + 2 \log \frac{2}{3}) \approx -0.48 \neq -\frac{r}{2} \log 2$ for any integer r . This creates an “irregular” value among other loss values of the form $-\frac{r}{2} \log 2$. In contrast, for pattern s_{1a} , the loss value of RS-GAN is $-\frac{1}{2} \min_{s,t} [\log(1 + e^{t-t}) + \log(1 + e^{t-s})] = -\frac{1}{2} \log 2$, which is of the form $-\frac{r}{2} \log 2$. Therefore, for the 2-point case, RS-GAN has a better landscape because it avoids the “irregular” value of JS-GAN due to its “pairing”. This insight is the foundation of the general theory presented in the next section.

4 Main Theoretical Results

4.1 Landscape Results in Function Space

We present our main theoretical results, extending the landscape results from $n = 2$ to general n .

Denote $\xi(m) \triangleq \sup_{t \in \mathbb{R}} (h_1(t) + mh_2(-t))$.

Assumption 4.1. $\sup_{t \in \mathbb{R}} h_1(t) = \sup_{t \in \mathbb{R}} h_2(t) = 0$.

Assumption 4.2. $\xi(m) > m\xi(1)$, $\forall m \in [2, n]$.

Assumption 4.3. $\xi(m) < \xi(m - 1)$, $\forall m \in [1, n]$.

It is easy to prove that under Assumption 4.1, $\xi(m - 1) \geq \xi(m) \geq m\xi(1)$ always holds. Assumption 4.2 and Assumption 4.3 require strict inequalities, thus do not always hold (e.g., for constant functions). Nevertheless, most non-constant functions satisfy these assumptions.

The separable-GAN (SepGAN) problem (empirical loss, function space) is

$$\min_{Y \in \mathbb{R}^{d \times n}} g_{SP}(Y), \text{ where } g_{SP}(Y) = \frac{1}{2n} \sup_{f \in C(\mathbb{R}^d)} \sum_{i=1}^n [h_1(f(x_i)) + h_2(-f(y_i))]. \quad (5)$$

Theorem 1. *Suppose $x_1, x_2, \dots, x_n \in \mathbb{R}^d$ are distinct. Suppose h_1, h_2 satisfy Assumptions 4.1, 4.2 and 4.3. Then for separable-GAN loss $g_{SP}(Y)$ defined in Eq. (5), we have: (i) The global minimal value is $-\frac{1}{2} \sup_{t \in \mathbb{R}} (h_1(t) + h_2(-t))$, which is achieved iff $\{y_1, \dots, y_n\} = \{x_1, \dots, x_n\}$. (ii) If $y_i \in \{x_1, \dots, x_n\}$, $i \in \{1, 2, \dots, n\}$ and $y_i = y_j$ for some $i \neq j$, then Y is a sub-optimal strict local minimum. Therefore, $g_{SP}(Y)$ has $(n^n - n!)$ sub-optimal strict local minima.*

Remark 1: $h_1(t) = h_2(t) = -\log(1 + e^{-t})$ satisfy Assumptions 4.1, 4.2 and 4.3, thus Theorem 1 applies to JS-GAN. It also applies to hinge-GAN with $h_1(t) = h_2(t) = -\max\{0, 1 - t\}$ and LS-GAN (least-square GAN) with $h_1(t) = -(1 - t)^2$, $h_2(t) = -t^2$.

Next we consider RpGANs. The RpGAN problem (empirical loss, function space) is

$$\min_{Y \in \mathbb{R}^{d \times n}} g_R(Y), \text{ where } g_R(Y) = \frac{1}{n} \sup_{f \in C(\mathbb{R}^d)} \sum_{i=1}^n [h(f(x_i) - f(y_i))]. \quad (6)$$

Definition 4.1. (*global-min-reachable*) We say a point w is global-min-reachable for a function $F(w)$ if there exists a continuous path from w to one global minimum of F along which the value of $F(w)$ is non-increasing.

Assumption 4.4. $\sup_{t \in \mathbb{R}} h(t) = 0$ and $h(0) < 0$.

Assumption 4.5. h is a concave function in \mathbb{R} .

Theorem 2. Suppose $x_1, x_2, \dots, x_n \in \mathbb{R}^d$ are distinct. Suppose h satisfies Assumptions 4.4 and 4.5. Then for RpGAN loss $g_{\mathbb{R}}$ defined in Eq. (6): (i) The global minimal value is $h(0)$, which is achieved iff $\{y_1, \dots, y_n\} = \{x_1, \dots, x_n\}$. (ii) Any Y is global-min-reachable for the function $g_{\mathbb{R}}(Y)$.

This result sanity checks the loss $g_{\mathbb{R}}(Y)$: its global minimizer is indeed the desired empirical distribution. In addition, it establishes a significantly different optimization landscape for RpGAN.

Remark 1: $h(t) = -\log(1 + e^{-t})$ satisfies Assumption 4.4 and 4.5, thus Theorem 2 applies to RS-GAN. It also applies to Rp-hinge-GAN with $h(t) = -\max\{0, a - t\}$ and Rp-LS-GAN with $h(t) = -(a - t)^2$, for any positive constant a .

Remark 2: The W-GAN loss is $\frac{1}{n} \sup_f \sum_i h(f(x_i) - f(y_i))$ where $h(t) = t$; however, since $\sup_t h(t) = \infty$ it does not satisfy Assumption 4.4. The unboundedness of $h(t) = t$ necessitates extra constraints, which make the landscape analysis of W-GAN challenging; see Appendix L. Analyzing the landscape of W-GAN is an interesting future work.

To prove Theorem 1, careful computation suffices; see Appendix I. The proof of Theorem 2 is a bit involved. We first build a graph with nodes representing x_i 's and y_i 's, then decompose the graph into cycles and trees, and finally compute the loss value by grouping the terms according to cycles and trees and calculate the contribution of each cycle and tree. The detailed proof is given in Appendix J.

4.2 Landscape Results in Parameter Space

We now consider a deep net generator G_w with $w \in \mathbb{R}^K$ and a deep net discriminator f_{θ} with $\theta \in \mathbb{R}^J$. Different from before, where we optimize over y_i and f (function space), we now optimize over w and θ (parameter space).

We first present a technical assumption. For $Z = (z_1, \dots, z_n) \in \mathbb{R}^{d_z \times n}$, $Y = (y_1, \dots, y_n) \in \mathbb{R}^{d_y \times n}$ and $\mathcal{W} \subseteq \mathbb{R}^K$, define a set $G^{-1}(Y; Z, \mathcal{W}) \triangleq \{w \in \mathcal{W} \mid G_w(z_i) = y_i, \forall i\}$.

Assumption 4.6. (path-keeping property of generator net): For any distinct $z_1, \dots, z_n \in \mathbb{R}^{d_z}$, any continuous path $Y(t), t \in [0, 1]$ in the space $\mathbb{R}^{d_y \times n}$ and any $w_0 \in G^{-1}(Y(0); Z, \mathcal{W})$, there is continuous path $w(t), t \in [0, 1]$ such that $w(0) = w_0$ and $Y(t) = G_{w(t)}(Z), t \in [0, 1]$.

Intuitively, this assumption relates the paths in the function space to the paths in the parameter space, thus the results in function space can be transferred to the results in parameter space. The formal results involve two extra assumptions on representation power of f_{θ} and G_w (see Appendix K for details). Informal results are as follows:

Proposition 1. (informal) Consider the separable-GAN problem $\min_{w \in \mathbb{R}^K} \varphi_{\text{sep}}(w)$, where

$$\varphi_{\text{sep}}(w) = \sup_{\theta} \frac{1}{2n} \sum_{i=1}^n [h_1(f_{\theta}(x_i)) + h_2(-f_{\theta}(G_w(z_i)))]. \quad (7)$$

Suppose h_1, h_2 satisfy the assumptions of Theorem 1. Suppose G_w satisfies Assumption 4.6 (with certain \mathcal{W}). Suppose f_{θ} and G_w have enough representation power (formalized in Appendix K). Then there exist at least $(n^n - n!)$ distinct $w \in \mathcal{W}$ that are not global-min-reachable for $\varphi_{\text{sep}}(w)$.

Proposition 2. (informal) Consider the RpGAN problem $\min_{w \in \mathbb{R}^K} \varphi_{\mathbb{R}}(w)$, where

$$\varphi_{\mathbb{R}}(w) = \sup_{\theta} \frac{1}{n} \sum_{i=1}^n [h(f_{\theta}(x_i)) - f_{\theta}(G_w(z_i))]. \quad (8)$$

Suppose h satisfies the assumptions of Theorem 2. Suppose G_w and f_{θ} satisfy the same assumptions as Proposition 1. Then any $w \in \mathcal{W}$ is global-min-reachable for $\varphi_{\mathbb{R}}(w)$.

Remark 1: The existence of a decreasing path does not necessarily mean an algorithm can follow it. Nevertheless, our results already distinguish SepGAN and RpGAN. We will illustrate that these results can improve our understanding of GAN training in Sec. 5, and present experiments supporting our theory in Sec. 6.

Remark 2: The two results rely on a few assumptions of neural-nets including Assumption 4.6. These assumptions can be satisfied by certain over-parameterized neural-nets, in which case \mathcal{W} is a certain dense subset of \mathbb{R}^K or \mathbb{R}^K itself. For details see Appendix K.1.

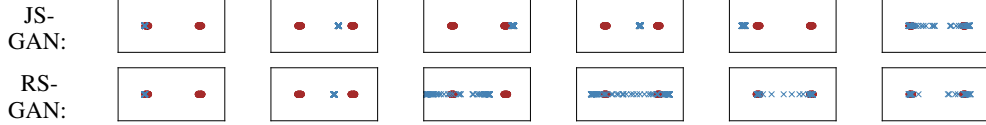


Figure 5: Training process of JS-GAN and RS-GAN for two-cluster data. True data are red, fake data are blue. RS-GAN escapes from mode collapse faster than JS-GAN.

4.3 Discussion of Implications

These results distinguish the SepGAN and RpGAN landscapes. Theoretically, there is evidence regarding the benefit of losses without sub-optimal basins. Bovier et al. [17] proved that it takes the Langevin diffusion at least $e^{\omega(h)}$ time to escape a depth- h basin. A recent work [91] proved that the hitting time of SGLD (stochastic gradient Langevin dynamics) is positively related to the height of the barrier, and SGLD may escape basins with low barriers relatively fast. The theoretical insight is that a landscape without a bad basin permits better quality solutions or a faster convergence to good-quality solutions.

We now discuss the possible gap between our theory and practice. We proved that a mode collapse Y^* is a bad basin in the generator space, which indicates that $(Y^*, D^*(Y^*))$ is an attractor in the joint space of (Y, D) and hard to escape by gradient descent ascent (GDA). In GAN training, the dynamics are not the same as GDA dynamics due to various reasons (e.g., sampling, unequal D and G updates), and basins could be escaped with enough training time (e.g., [91]). In addition, a randomly initialized (Y, D) might be far away from the basins at $(Y^*, D^*(Y^*))$, and properly chosen hyper-parameters (e.g., learning rate) may re-position the dynamics so as to avoid attraction to bad basins. Further, it is known that adding neurons can smooth the landscape of deep nets (e.g., eliminating bad basins in neural-nets [50]), thus wide nets might help escape basins in the (Y, D) -space faster. In short, the effect of bad basins may be mitigated via the following factors: (i) proper initial D and Y ; (ii) long enough training time; (iii) wide neural-nets; (iv) enough hyper-parameter tuning. These factors make it relatively hard to detect the existence of bad basins and their influences. We support our landscape theory, by identifying differences of SepGAN and RpGAN in synthetic and real-data experiments.

5 Case Study of Two-Cluster Experiments

Although in Section 3 we argue that, *intuitively*, mode collapse can happen for training JS-GAN for two-point generation, it does not necessarily mean mode collapse really appears in practical training. We discuss a two-cluster experiment, an extension of two-point generation, in order to build a link between theory and practice. We aim to understand the following question: does mode collapse really appear as a “basin”, and how does it affect training?

Suppose the true data are two clusters around $c_1 = 0$ and $c_2 = 4$. We sample 100 points from the two clusters as x_i 's, and sample z_1, \dots, z_{100} uniformly from an interval. We use 4-layer neural-nets for the discriminator and generator. We use the non-saturating versions of JS-GAN and RS-GAN.

Mode collapse as bad basin can appear. We visualize the movement of fake data in Fig. 5, and plot the loss value of D (indicating the discriminator) over iterations in Fig. 6(a,b). Interestingly, the minimal D losses are around 0.48, which is the value of ϕ_{JS} at state s_{1a} . It is easy to check that the optimal $D = D^*(s_{1a})$ for a mode collapse state s_{1a} satisfies $\{D(c_1), D(c_2)\} = \{1, 1/3\}$, and Fig. 6(c) shows that at iteration 2800 the D actually becomes D^* . This provides a concrete example that training gets stuck at a mode collapse due to the bad-basin-effect. We also notice that there are a few more attempts to approach the bad attractor $(s_{1a}, D^*(s_{1a}))$ (e.g., from iteration 2000 to 2500). In RS-GAN training, the minimal loss is around 0.35, which is also the value of ϕ_{RS} at state s_{1a} . The attracting power of $(s_{1a}, D^*(s_{1a}))$ is weaker than for JS-GAN. Thus it only attracts the iterates for a very short time. RS-GAN needs 800 iterations to escape, which is about 3 times faster than the escape for JS-GAN.

Effect of width: We see a clear effect of width on convergence speed. As the networks become wider, both JS-GAN and RS-GAN converge faster. We find that the reason of faster convergence is because wider nets make JS-GAN escape mode collapse faster. See details in Appendix B.

More experiment details and findings are presented in Appendix B.

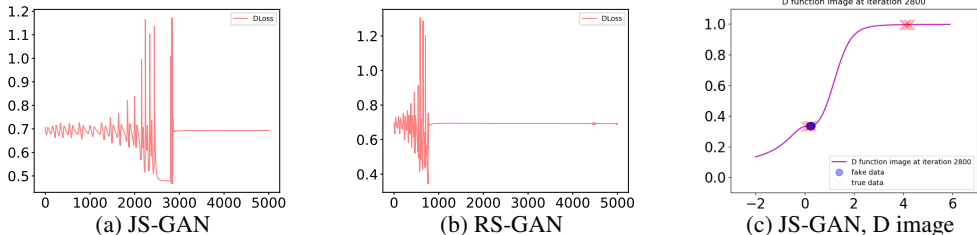


Figure 6: (a) and (b): Evolution of D loss over iterations. RS-GAN is 3-4 \times faster than JS-GAN. (c) For JS-GAN training in (a), we plot (Y, D) together at iteration 2800. Y are represented in blue points, and they are near $c_1 = 0$. D is near the optimal $D^*(s_{1a})$ since $D(0) \approx 1/3$ and $D(4) \approx 1$. Interestingly, this bad attractor (Y, D) is similar to the one discussed in Fig. 1, so the intuition of “local-min” is verified in (c).

	CIFAR-10				STL-10			
	Inception Score \uparrow	FID \downarrow	FID Gap	Model size	Inception Score \uparrow	FID \downarrow	FID Gap	Model size
Real Dataset	11.24 \pm 0.19	5.18			24.45 \pm 0.41	5.34		
Standard CNN								
WGAN-GP	6.68 \pm 0.06	39.66			8.11 \pm 0.09	55.64		
JS-GAN	6.27 \pm 0.10	49.13	15.34	100%	8.01 \pm 0.07	50.38		
RS-GAN	7.02 \pm 0.07	33.79			7.62 \pm 0.08	52.54	2.16	100%
JS-GAN+ SN	7.42 \pm 0.08	28.07	0.91	100%	8.32 \pm 0.10	44.06	0.18	100%
RS-GAN+ SN	7.32 \pm 0.08	27.16			8.29 \pm 0.13	43.88		
JS-GAN+SN; GD channel/2	6.85 \pm 0.08	33.90	1.16	29.0%	7.69 \pm 0.05	57.16	4.69	32.9%
RS-GAN+SN; GD channel/2	6.74 \pm 0.04	32.74			7.95 \pm 0.10	52.47		
JS-GAN + SN; GD channel/4	5.83 \pm 0.07	52.63	7.26	9.2%	6.90 \pm 0.06	72.96	9.35	11.9%
RS-GAN + SN; GD channel/4	5.94 \pm 0.09	45.37			7.27 \pm 0.11	63.61		
ResNet								
JS-GAN+ SN	8.12 \pm 0.14	20.13	0.82	100%	8.87 \pm 0.07	36.33	1.56	100%
RS-GAN + SN	7.92 \pm 0.13	19.31			8.96 \pm 0.10	34.77		
JS-GAN + SN; GD channel/2	7.67 \pm 0.04	23.29	1.51	27.5%	8.45 \pm 0.05	44.39	2.21	29.0%
RS-GAN + SN; GD channel/2	7.63 \pm 0.07	21.78			8.47 \pm 0.09	42.18		
JS-GAN + SN; GD channel/4	6.65 \pm 0.06	45.20	13.94	10.4%	8.21 \pm 0.12	53.57	1.48	9.2%
RS-GAN+ SN; GD channel/4	7.08 \pm 0.05	31.26			8.46 \pm 0.11	52.09		
JS-GAN + SN; BottleNeck	7.60 \pm 0.07	26.98	1.54	16.8%	8.29 \pm 0.05	50.38	3.80	19.2%
RS-GAN+ SN; BottleNeck	7.57 \pm 0.09	25.44			8.52 \pm 0.11	46.58		

Table 2: Inception score (IS) (higher is better) and Frechét Inception distance (FID) (lower is better) for JS-GAN, WGAN-GP and RS-GAN on CIFAR-10 and STL-10. We also show FID gap between JS-GAN and RS-GAN, and show the relative model size of narrow nets vs. regular nets (“regular”: CNN and ResNet of [67]).

6 Real Data Experiments

RpGANs have been tested by Jolicoeur-Martineau [41], and are shown to be better than their SepGAN counterparts in a variety of settings⁴. In addition, RpGAN and its variants have been used in super-resolution (ESRGAN) [85] and a few recent GANs [87, 13]. Therefore, the effectiveness of RpGANs has been justified to some extent. We do not attempt to re-run the experiments merely for the purpose of justification. Instead, our goal is to use experiments to support our landscape theory.

Based on the discussions in Sec. 2, Sec. 4 and Sec. 5, we conjecture that RpGANs have a bigger advantage over SepGAN (A) with narrow deep nets, (B) in high resolution image generation, (C) with imbalanced data. Finally, (D) there exists some bad initial D that makes SepGANs much worse than RpGANs. In the main text, we present results on the logistic loss (i.e., JS-GAN and RS-GAN). Results on other losses are given in the appendix.

Experimental setting for (A). For (A), we test on CIFAR-10 and STL-10 data. For the optimizer, we use Adam with the discriminator’s learning rate 0.0002. For CIFAR-10 on ResNet, we set $\beta_1 = 0$ and $\beta_2 = 0.9$ in Adam; for others, $\beta_1 = 0.5$ and $\beta_2 = 0.999$. We tune the generator’s learning rate and run 100k iterations in total. We report the Inception score (IS) and Frechét Inception distance (FID). IS and FID are evaluated on 50k and 10k samples respectively. More details of the setting are shown in Appendix E.1, and the experimental settings for other cases besides (A) are shown in the corresponding parts in the appendix. Generated images are shown in Appendix F.

Regular architecture and effect of spectral norm (SN). We use the two neural architectures in [67]: standard CNN and ResNet, and report results in Table 2. First, without spectral normalization (SN), RS-GAN achieves much higher accuracy than JS-GAN and WGAN-GP on CIFAR-10. Second, with

⁴That paper tested a number of variants, and some of them are not directly covered by our results.

SN, RS-GAN achieves 1-2 points lower FID score than JS-GAN, i.e., it’s slightly better. We suspect that SN smoothens the landscape, thus greatly reducing the gap between JS-GAN and RS-GAN. Note that the scores of JS-GAN and WGAN-GP (both without and with SN) are comparable to or better than the scores in Table 2 of Miyato et al. [67].

Narrow nets. For both CNN and ResNet, we reduce the number of channels for all convolutional layers in the generator and discriminator to (1) half, (2) quarter and (3) bottleneck (for ResNet structure). The experimental results are provided in Table 2. We consider the gap between RS-GAN and JS-GAN for regular width as a baseline. For narrow nets, the gap between RS-GAN and JS-GAN is similar or larger in most cases, and can be much larger (e.g. > 13 FID) in some cases. The fluctuations in the gaps are consistent with landscape theory: if JS-GAN training gets stuck at a bad basin then the performance is bad; if it converges to a good basin, then the performance is reasonably good. In CIFAR-10, compared to SN-GAN with the conventional ResNet (FID=20.13), we can achieve a relatively close result by using RS-GAN with 28% parameters (half channel, FID=21.78).

High resolution data experiments. Sec. 2 discusses that the non-convexity of JS-GAN will become a more severe issue when the number of samples is limited compared to the data space (e.g., high resolution space or limited data points). We conduct experiments with LSUN Church and Tower images of size 256×256 . RS-GAN can generate higher visual quality images than JS-GAN (Appendix F). Similarly, using another model architecture, [41] achieves a better FID score with RSGAN on the CAT dataset, which contains a small number of images (e.g., 2k 256×256 images).

Imbalanced data experiments. For imbalanced data, we find more evidence for the existence of JS-GAN’s bad basins. The reason: JS-GAN would have a deeper bad basin, and hence a higher chance to get stuck. We conduct ablation experiments on 2-cluster data and MNIST. Both cases show that JS-GAN ends up with mode collapse while RS-GAN can generate data with proportions similar to the imbalanced true data. Check Appendix C for more.

Bad initial point experiments. A better landscape is more robust to initialization. On MNIST data, we find a discriminator (not random) which permits RS-GAN to converge to a much better solution than JS-GAN when used as the starting point. The FID scores are reported in the table to the right. The gap is at least 30 FID scores (a much higher gap than the gap for a random initialization). Check Appendix D for more.

JS-GAN	65	78	60	93	139	137
RSGAN	29	30	30	26	32	56
	5e-01	1e-06	5e-06	1e-05	5e-05	1e-04

generator lr = discriminator lr

Combining with EMA. It is known that non-convergence can be alleviated via EMA [88], and our theory predicts that the global landscape issue can be alleviated by RpGAN. Non-convergence and global landscape are orthogonal: no matter whether iterates are near a sub-optimal local basin or a globally-optimal basin, the algorithm may cycle. Therefore, we conjecture that the effect of EMA and the effect of RS-GAN are “additive”. Our simulations show that EMA can improve both JS-GAN and RS-GAN, and the gap is approximately preserved after adding EMA. Combining EMA and RS-GAN, we achieve a similar result to the baseline (JS-GAN + SN, no EMA, FID = 20.13) using 16.8% parameters (Resnet with bottleneck plus EMA, FID=21.38). See Appendix E.1 for more.

General RpGAN: We conduct additional experiments on other losses, including hinge loss and least squares loss. See Appendix E.2 and E.3 for more.

7 Conclusion

Global optimization landscape, together with statistical analysis and convergence analysis, are important theoretical angles. In this work, we study the global landscape of GANs. Our major questions are: (1) Does the original JS-GAN formulation have a good landscape? (2) If not, is there a simple way to improve the landscape in theory? (3) Does the improved landscape lead to better performance? First, studying the empirical versions of SepGAN (extension of JS-GAN) we prove that it has exponentially many bad basins, which are mode-collapse patterns. Second, we prove that a simple coupling idea (resulting in RpGAN) can remove bad basins in theory. Finally, we verify a few predictions based on the landscape theory, e.g., RS-GAN has a bigger advantage over JS-GAN for narrow nets.

Acknowledgements

This work is supported in part by NSF under Grant # 1718221, 2008387, 1755847 and MRI #1725729, and NIFA award 2020-67021-32799. We thank Sewoong Oh for pointing out the connection of the earlier version of our work to [41].

References

- [1] J. Adler and S. Lunz. Banach wasserstein gan. In *NeurIPS*, 2018.
- [2] Z. Allen-Zhu, Y. Li, and Z. Song. A convergence theory for deep learning via over-parameterization. In *ICML*, 2019.
- [3] M. Arjovsky and L. Bottou. Towards principled methods for training generative adversarial networks. In *ICLR*, 2017.
- [4] M. Arjovsky, S. Chintala, and L. Bottou. Wasserstein gan. In *ICML*, 2017.
- [5] S. Arora, R. Ge, Y. Liang, T. Ma, and Y. Zhang. Generalization and equilibrium in generative adversarial nets (GANs). In *ICML*, 2017.
- [6] W. Azizian, I. Mitliagkas, S. Lacoste-Julien, and G. Gidel. A tight and unified analysis of extragradient for a whole spectrum of differentiable games. *arXiv preprint arXiv:1906.05945*, 2019.
- [7] Y. Bai, T. Ma, and A. Risteski. Approximability of discriminators implies diversity in gans. *arXiv preprint arXiv:1806.10586*, 2018.
- [8] D. Balduzzi, S. Racaniere, J. Martens, J. Foerster, K. Tuyls, and T. Graepel. The mechanics of n-player differentiable games. *arXiv preprint arXiv:1802.05642*, 2018.
- [9] P. L. Bartlett, D. J. Foster, and M. J. Telgarsky. Spectrally-normalized margin bounds for neural networks. In *NeurIPS*, 2017.
- [10] Y. Bengio and Y. LeCun. Scaling learning algorithms towards AI. In *Large Scale Kernel Machines*. MIT Press, 2007.
- [11] H. Berard, G. Gidel, A. Almahairi, P. Vincent, and S. Lacoste-Julien. A closer look at the optimization landscapes of generative adversarial networks. *arXiv preprint arXiv:1906.04848*, 2019.
- [12] D. Berthelot, T. Schumm, and L. Metz. Began: Boundary equilibrium generative adversarial networks. *arXiv preprint arXiv:1703.10717*, 2017.
- [13] D. Berthelot, P. Milanfar, and I. Goodfellow. Creating high resolution images with a latent adversarial generator. *arXiv preprint arXiv:2003.02365*, 2020.
- [14] S. Bhojanapalli, B. Neyshabur, and N. Srebro. Global optimality of local search for low rank matrix recovery. In *NeurIPS*, 2016.
- [15] M. Bianchini and M. Gori. Optimal learning in artificial neural networks: A review of theoretical results. *Neurocomputing*, 1996.
- [16] M. Bińkowski, D. J. Sutherland, M. Arbel, and A. Gretton. Demystifying mmd gans. In *ICLR*, 2018.
- [17] A. Bovier, M. Eckhoff, V. Gayrard, and M. Klein. Metastability in reversible diffusion processes i. sharp asymptotics for capacities and exit times. *JEMS*, 2004.
- [18] A. Brock, J. Donahue, and K. Simonyan. Large scale gan training for high fidelity natural image synthesis. *arXiv preprint arXiv:1809.11096*, 2018.
- [19] Y. Chi, Y. M. Lu, and Y. Chen. Nonconvex optimization meets low-rank matrix factorization: An overview. *IEEE Transactions on Signal Processing*, 67(20):5239–5269, 2019.
- [20] C. Chu, J. Blanchet, and P. Glynn. Probability functional descent: A unifying perspective on gans, variational inference, and reinforcement learning. *arXiv preprint arXiv:1901.10691*, 2019.
- [21] R. W. A. Cully, H. J. Chang, and Y. Demiris. Magan: Margin adaptation for generative adversarial networks. *arXiv preprint arXiv:1704.03817*, 2017.

- [22] C. Daskalakis and I. Panageas. The limit points of (optimistic) gradient descent in min-max optimization. In *NeurIPS*, 2018.
- [23] C. Daskalakis, A. Ilyas, V. Syrgkanis, and H. Zeng. Training gans with optimism. In *ICLR*, 2018.
- [24] I. Deshpande, Z. Zhang, and A. Schwing. Generative modeling using the sliced wasserstein distance. In *CVPR*, 2018.
- [25] I. Deshpande, Y.-T. Hu, R. Sun, A. Pyrros, N. Siddiqui, S. Koyejo, Z. Zhao, D. Forsyth, and A. G. Schwing. Max-Sliced Wasserstein Distance and its use for GANs. In *CVPR*, 2019.
- [26] T. Ding, D. Li, and R. Sun. Sub-optimal local minima exist for almost all over-parameterized neural networks. *arXiv preprint arXiv:1911.01413*, 2019.
- [27] S. S. Du, J. D. Lee, H. Li, L. Wang, and X. Zhai. Gradient descent finds global minima of deep neural networks. *arXiv preprint arXiv:1811.03804*, 2018.
- [28] F. Farnia and A. Ozdaglar. Gans may have no nash equilibria. *arXiv preprint arXiv:2002.09124*, 2020.
- [29] F. Farnia and D. Tse. A convex duality framework for gans. In *NeurIPS*, 2018.
- [30] S. Feizi, F. Farnia, T. Ginart, and D. Tse. Understanding gans: the lqg setting. *arXiv preprint arXiv:1710.10793*, 2017.
- [31] R. Ge, J. D. Lee, and T. Ma. Matrix completion has no spurious local minimum. In *NeurIPS*, 2016.
- [32] M. Geiger, S. Spigler, S. d’Ascoli, L. Sagun, M. Baity-Jesi, G. Biroli, and M. Wyart. The jamming transition as a paradigm to understand the loss landscape of deep neural networks. *arXiv preprint arXiv:1809.09349*, 2018.
- [33] G. Gidel, H. Berard, G. Vignoud, P. Vincent, and S. Lacoste-Julien. A variational inequality perspective on generative adversarial networks. *arXiv preprint arXiv:1802.10551*, 2018.
- [34] G. Gidel, R. A. Hemmat, M. Pezeshki, R. Lepriol, G. Huang, S. Lacoste-Julien, and I. Mitliagkas. Negative momentum for improved game dynamics. In *AISTATS*, 2019.
- [35] I. Goodfellow, J. Pouget-Abadie, M. Mirza, B. Xu, D. Warde-Farley, S. Ozair, A. Courville, and Y. Bengio. Generative adversarial nets. In *NeurIPS*, 2014.
- [36] I. Gulrajani, F. Ahmed, M. Arjovsky, V. Dumoulin, and A. Courville. Improved training of wasserstein gans. In *NeurIPS*, 2017.
- [37] X. Huang, Y. Li, O. Poursaeed, J. Hopcroft, and S. Belongie. Stacked generative adversarial networks. In *CVPR*, 2017.
- [38] A. Jacot, F. Gabriel, and C. Hongler. Neural tangent kernel: Convergence and generalization in neural networks. In *NeurIPS*, 2018.
- [39] C. Jin, P. Netrapalli, and M. I. Jordan. Minmax optimization: Stable limit points of gradient descent ascent are locally optimal. *arXiv preprint arXiv:1902.00618*, 2019.
- [40] R. Johnson and T. Zhang. A framework of composite functional gradient methods for generative adversarial models. *IEEE transactions on pattern analysis and machine intelligence*, 2019.
- [41] A. Jolicoeur-Martineau. The relativistic discriminator: a key element missing from standard gan. In *ICLR*, 2018.
- [42] A. Jolicoeur-Martineau. On relativistic f-divergences. In *ICML*, 2019.
- [43] T. Karras, S. Laine, and T. Aila. A style-based generator architecture for generative adversarial networks. In *Proceedings of the IEEE conference on computer vision and pattern recognition*, pages 4401–4410, 2019.
- [44] T. Karras, S. Laine, M. Aittala, J. Hellsten, J. Lehtinen, and T. Aila. Analyzing and improving the image quality of stylegan. In *Proceedings of the IEEE/CVF Conference on Computer Vision and Pattern Recognition*, pages 8110–8119, 2020.
- [45] N. Kodali, J. Abernethy, J. Hays, and Z. Kira. On convergence and stability of gans. *arXiv preprint arXiv:1705.07215*, 2017.

- [46] S. Kolouri, C. E. Martin, and G. K. Rohde. Sliced-wasserstein autoencoder: An embarrassingly simple generative model. *arXiv preprint arXiv:1804.01947*, 2018.
- [47] J. Lee, L. Xiao, S. Schoenholz, Y. Bahri, R. Novak, J. Sohl-Dickstein, and J. Pennington. Wide neural networks of any depth evolve as linear models under gradient descent. In *Advances in neural information processing systems*, pages 8572–8583, 2019.
- [48] Q. Lei, J. D. Lee, A. G. Dimakis, and C. Daskalakis. Sgd learns one-layer networks in wgens. *arXiv preprint arXiv:1910.07030*, 2019.
- [49] C.-L. Li, W.-C. Chang, Y. Cheng, Y. Yang, and B. Póczos. Mmd gan: Towards deeper understanding of moment matching network. In *NeurIPS*, 2017.
- [50] D. Li, T. Ding, and R. Sun. Over-parameterized deep neural networks have no strict local minima for any continuous activations. *arXiv preprint arXiv:1812.11039*, 2018.
- [51] J. Li, A. Madry, J. Peebles, and L. Schmidt. On the limitations of first-order approximation in gan dynamics. *arXiv preprint arXiv:1706.09884*, 2017.
- [52] J. Li, A. Madry, J. Peebles, and L. Schmidt. Towards understanding the dynamics of generative adversarial networks. In *ICML*, 2018.
- [53] K. Li and J. Malik. Implicit maximum likelihood estimation. *arXiv preprint arXiv:1809.09087*, 2018.
- [54] Y. Li, A. G. Schwing, K.-C. Wang, and R. Zemel. Dualing GANs. In *NeurIPS*, 2017.
- [55] S. Liang, R. Sun, J. D. Lee, and R. Srikant. Adding one neuron can eliminate all bad local minima. In *Advances in Neural Information Processing Systems*, pages 4350–4360, 2018.
- [56] S. Liang, R. Sun, Y. Li, and R. Srikant. Understanding the loss surface of neural networks for binary classification. *arXiv preprint arXiv:1803.00909*, 2018.
- [57] S. Liang, R. Sun, and R. Srikant. Revisiting landscape analysis in deep neural networks: Eliminating decreasing paths to infinity. *arXiv preprint arXiv:1912.13472*, 2019.
- [58] Z. Lin, A. Khetan, G. Fanti, and S. Oh. Pacgan: The power of two samples in generative adversarial networks. In *NeurIPS*, 2018.
- [59] S. Liu and K. Chaudhuri. The inductive bias of restricted f-gans. *arXiv preprint arXiv:1809.04542*, 2018.
- [60] R. Livni, S. Shalev-Shwartz, and O. Shamir. On the computational efficiency of training neural networks. In *NeurIPS*, 2014.
- [61] A. V. Makkuva, A. Taghvaei, S. Oh, and J. D. Lee. Optimal transport mapping via input convex neural networks. *arXiv preprint arXiv:1908.10962*, 2019.
- [62] X. Mao, Q. Li, H. Xie, R. Y. K. Lau, Z. Wang, and S. P. Smolley. Least Squares Generative Adversarial Networks. *arXiv e-prints*, 2016.
- [63] X. Mao, Q. Li, H. Xie, R. Y. Lau, Z. Wang, and S. Paul Smolley. Least squares generative adversarial networks. In *ICCV*, 2017.
- [64] E. V. Mazumdar, M. I. Jordan, and S. S. Sastry. On finding local nash equilibria (and only local nash equilibria) in zero-sum games. *arXiv preprint arXiv:1901.00838*, 2019.
- [65] L. Mescheder, A. Geiger, and S. Nowozin. Which training methods for gans do actually converge? In *ICML*, 2018.
- [66] L. Metz, B. Poole, D. Pfau, and J. Sohl-Dickstein. Unrolled generative adversarial networks. In *ICLR*, 2017.
- [67] T. Miyato, T. Kataoka, M. Koyama, and Y. Yoshida. Spectral normalization for generative adversarial networks. In *ICLR*, 2018.
- [68] S. Mohamed and B. Lakshminarayanan. Learning in implicit generative models. *arXiv preprint arXiv:1610.03483*, 2016.
- [69] Y. Mroueh and T. Sercu. Fisher gan. In *NeurIPS*, 2017.
- [70] Y. Mroueh, T. Sercu, and V. Goel. MCGAN: Mean and covariance feature matching gan. *arXiv preprint arXiv:1702.08398*, 2017.

- [71] V. Nagarajan and J. Z. Kolter. Gradient descent gan optimization is locally stable. In *NeurIPS*, 2017.
- [72] Q. Nguyen and M. Hein. The loss surface of deep and wide neural networks. In *ICML*, 2017.
- [73] Q. Nguyen, M. C. Mukkamala, and M. Hein. On the loss landscape of a class of deep neural networks with no bad local valleys. *arXiv preprint arXiv:1809.10749*, 2018.
- [74] S. Nowozin, B. Cseke, and R. Tomioka. f-gan: Training generative neural samplers using variational divergence minimization. In *NeurIPS*, 2016.
- [75] B. Poole, A. A. Alemi, J. Sohl-Dickstein, and A. Angelova. Improved generator objectives for gans. *arXiv preprint arXiv:1612.02780*, 2016.
- [76] A. Radford, L. Metz, and S. Chintala. Unsupervised representation learning with deep convolutional generative adversarial networks. In *ICLR*, 2016.
- [77] S. J. Reddi, S. Kale, and S. Kumar. On the convergence of adam and beyond. In *ICLR*, 2018.
- [78] T. Salimans, I. Goodfellow, W. Zaremba, V. Cheung, A. Radford, X. Chen, and X. Chen. Improved techniques for training gans. In *NeurIPS*, 2016.
- [79] M. Sanjabi, J. Ba, M. Razaviyayn, and J. D. Lee. On the convergence and robustness of training gans with regularized optimal transport. In *NeurIPS*, 2018.
- [80] R. Sun, D. Li, S. Liang, T. Ding, and R. Srikant. The global landscape of neural networks: An overview. *IEEE Signal Processing Magazine*, 37(5):95–108, 2020.
- [81] R.-Y. Sun. Optimization for deep learning: An overview. *Journal of the Operations Research Society of China*, pages 1–46, 2020.
- [82] D. Tran, R. Ranganath, and D. M. Blei. Deep and hierarchical implicit models. In *NeurIPS*, 2017.
- [83] T. Unterthiner, B. Nessler, C. Seward, G. Klambauer, M. Heusel, H. Ramsauer, and S. Hochreiter. Coulomb gans: Provably optimal nash equilibria via potential fields. In *International Conference on Learning Representations*, 2018.
- [84] L. Venturi, A. S. Bandeira, and J. Bruna. Spurious valleys in two-layer neural network optimization landscapes. *arXiv preprint arXiv:1802.06384*, 2018.
- [85] X. Wang, K. Yu, S. Wu, J. Gu, Y. Liu, C. Dong, Y. Qiao, and C. Change Loy. Esrgan: Enhanced super-resolution generative adversarial networks. In *ECCV*, 2018.
- [86] J. Wu, Z. Huang, W. Li, J. Thoma, and L. Van Gool. Sliced wasserstein generative models. In *CVPR*, 2019.
- [87] Y. Xiangli, Y. Deng, B. Dai, C. C. Loy, and D. Lin. Real or not real, that is the question. *arXiv preprint arXiv:2002.05512*, 2020.
- [88] Y. Yazıcı, C.-S. Foo, S. Winkler, K.-H. Yap, G. Piliouras, and V. Chandrasekhar. The unusual effectiveness of averaging in gan training. In *ICLR*, 2019.
- [89] H. Zhang, I. Goodfellow, D. Metaxas, and A. Odena. Self-attention generative adversarial networks. In *ICML*, 2018.
- [90] J. Zhang, P. Xiao, R. Sun, and Z.-Q. Luo. A single-loop smoothed gradient descent-ascent algorithm for nonconvex-concave min-max problems. *arXiv preprint arXiv:2010.15768*, 2020.
- [91] Y. Zhang, P. Liang, and M. Charikar. A hitting time analysis of stochastic gradient langevin dynamics. *arXiv preprint arXiv:1702.05575*, 2017.
- [92] D. Zou, Y. Cao, D. Zhou, and Q. Gu. Stochastic gradient descent optimizes over-parameterized deep relu networks. *arXiv preprint arXiv:1811.08888*, 2018.

Appendix: Towards a Better Global Loss Landscape of GANs

The code is available at <https://github.com/AilsaF/RS-GAN>. This appendix consists of additional experiments, related work, proofs, other results and various discussions.

Contents

1	Introduction	1
2	Difference of Population Loss and Empirical Loss	2
3	Landscape Analysis of GANs: Intuition and Toy Results	3
4	Main Theoretical Results	5
4.1	Landscape Results in Function Space	5
4.2	Landscape Results in Parameter Space	6
4.3	Discussion of Implications	7
5	Case Study of Two-Cluster Experiments	7
6	Real Data Experiments	8
7	Conclusion	9
A	Related Work	15
A.1	Related Works on Local Minima and Mode Collapse	15
B	2-Cluster Experiments: Details and More Discussions	17
C	Result and Experiments for Imbalanced Data Distribution	18
C.1	Imbalanced Data: Math Results for Two-Clusters	18
C.2	Experiments	19
D	Experiments of Bad Initialization	19
E	Experiments of Regular Training: More Details and More Results	20
E.1	Experiment Details and More Experiments with Logistic Loss	20
E.2	Experiments with Hinge Loss	22
E.3	Experiments with Least Square Loss	22
F	Experiments on High Resolution Data	22
G	Discussions on Empirical Loss and Population Loss (complements Sec. 2)	23
G.1	Particle space or probability space?	23
G.2	Empirical loss and population loss	24
G.3	Generalization and overfitting of GAN	24
H	Proofs for Section 3 (2-Point Case) and Appendix C (2-Cluster Case)	24
H.1	Proof of Claim 3.1 and Corollary 3.1 (for JS-GAN)	24
H.2	Proof of Claim 3.2 (for RS-GAN)	25
H.3	Proofs for 2-Cluster Data (Possibly Imbalanced)	26
I	Proof of Theorem 1 (Landscape of Separable-GAN)	26
J	Proof of Theorem 2 (Landscape of RpGAN)	27
J.1	Warm-up Example	27
J.2	Proof of Theorem J.1	28
J.2.1	Graph Preliminaries and Proof of Lemma 1	30
J.2.2	Proof of Claim J.1	31
J.3	Proof of Theorem 2	32
K	Results in Parameter Space	33
K.1	Sufficient Conditions for the Assumptions	33
K.2	Other Sufficient Conditions	34
K.3	Proofs of Propositions for Parameter Space	35
K.4	A technical lemma	36
K.5	Proof of claims	37
L	Discussion of Wasserstein GAN	37

A Related Work

We provide a more detailed overview of related work in this section.

Global analysis in supervised learning. Recently, global landscape analysis has attracted much attention. See Sun [81], Sun et al. [80], Bianchini and Gori [15] for surveys and [55, 57, 26, 56, 38, 2, 92, 27] for some recent works. It is widely believed that wide networks have a nice loss landscape and thus local minima are less of a concern (e.g., [60, 32, 50]). However, this claim only holds for supervised learning, and it is not clear whether local minima cause training difficulties for GANs.

Single-mode analysis. For single-mode data, Feizi et al. [30] and Mescheder et al. [65] provide a global analysis of GANs. They consider a single point 0 and a single Gaussian respectively. Feizi et al. [30] differs from ours in a few aspects. First, they consider the single-mode setting which does not have an issue of mode collapse. Second, they assume p_{data} is a Gaussian distribution, while we consider an arbitrary empirical distribution. Third, they analyze “quadratic-GAN,” which is not common in practice, while we analyze commonly used GAN formulations (including JS-GAN).

Mode collapse. Mode collapse is one of the major challenges for GANs which received a lot of attention. There are a few high-level hypotheses, such as improper loss functions [3, 5] and weak discriminators [66, 78, 5, 52]. Interestingly, RpGAN both changes the loss function and improves the discriminator. The theoretical analysis of mode collapse is relatively scarce. Lin et al. [58] makes a key observation that two distributions with the same total variation (TV) distance to true distribution do not exhibit the same degree of mode collapse. They proposed to pack the samples (PacGAN) to alleviate mode collapse. This work is rather different from ours. First, they analyze the TV distance, while we analyzed SepGANs and RpGANs. Second, their analysis is statistical, while our analysis is about optimization. As for the empirical guidance, RpGAN and PacGAN are complimentary and can be used together (suggested by the author of [41]). There are a few more works that discuss mode collapse and/or local minima; we defer the discussion to Appendix A.1.

Theoretical studies of loss functions. The early work on GANs [35] built a link between the min-max formulation and the J-S distance to justify the formulation. Arjovsky and Bottou [3] pointed out some possible drawbacks of J-S distance, and proposed a new loss based on Wasserstein distance, referred to as WGAN. Later, Arora et al. [5] point out that both Wasserstein distance and J-S distance are not generalizable, but they also argued that this is not too scary since people are not directly minimizing these two distances but a class of metrics referred to as “neural-network distance.”

Convergence analysis. Many recent works analyze convergence of GANs and/or min-max optimization, e.g., [23, 22, 6, 34, 64, 88, 39, 79, 90]. These works often only analyze local stability or convergence to local minima (or stationary points), making it different from our work. Lei et al. [48] studied the convergence of WGAN, but restricted to 1-layer neural nets.

Other theoretical analysis. There are a few other theoretical analysis of GANs, e.g., [68, 59, 29, 16, 8, 51, 61, 48]. Most of these works are not directly related to our work.

Other GAN Variants. There are many GAN variants, e.g., WGAN [4, 3, 36] and variants [86, 46, 1, 24, 25], f -GAN [74], SN-GAN [67], self-attention GAN [89], StyleGAN [43, 44] and many more [63, 69, 12, 70, 21, 54, 49, 78, 74, 75, 66, 37, 76, 10, 49]. Our analysis framework (analyzing global landscape of empirical loss) can potentially be applied to more variants mentioned above.

A.1 Related Works on Local Minima and Mode Collapse

We discuss a few related works on local minima and mode collapse, including Kodali et al. [45], Li and Malik [53] and Unterthiner et al. [83] that are mentioned in the main text.

DRAGAN. Kodali et al. [45] suggested the connection between mode collapse and a bad equilibrium based on the following empirical observation: a sudden increase of the gradient norm of the discriminator during training is associated with a sudden drop of the IS score. However, Kodali et al. [45] don’t present formal theoretical results on the relation between mode collapse and a bad equilibrium.

IMLE. Li and Malik [53] proposed implicit maximum likelihood estimation (IMLE). The empirical version of IMLE in the parameter space is the following:

$$\min_w \sum_{j=1}^n \min_{i \in \{1, \dots, m\}} \|x_i - G_w(z_j)\|^2. \tag{9}$$

In other words, for each generated sample $y_j = G_w(z_j)$, the loss is the distance from y_j to the closest true sample x_i . Interestingly, IMLE and RpGAN both couple the true data and the fake data in the loss. The differences are two fold: first, IMLE does not have an extra discriminator f_θ , while RpGAN has; second, IMLE compares y_j with all x_i (so as to find the nearest neighbor) while RpGAN compares y_j with an arbitrary x_j . See Table 3 for a comparison. Note that Li and Malik [53] don't present formal theoretical results on the landscape.

Table 3: Models that couple true data and fake data in the loss

Model name	Empirical form of loss ⁱ	Form of coupling	Optimization
RpGAN [41]	$\max_f \sum_j h(f(x_j) - f(y_j))$	pairing	min-max ⁱⁱ
RaGAN ⁱⁱⁱ [41]	$\max_f \sum_j h(\frac{1}{n} \sum_{i=1}^n f(x_i) - f(y_j))$	comparing with average	min-max
(max-)sliced-WGAN [24, 25]	$\max_{ f _L \leq 1} \sum_{i=1}^n [f(X)_{(i)} - f(Y)_{(i)}]^2$ ^{iv}	pairing sorted output	min-max
IMLE [53]	$\sum_j \min_{i \in [n]} \ y_j - x_i\ ^2$	comparing with closest	min
Coulomb-GAN [83]	$\sum_{i,j} k(x_i, x_j) + \sum_{i,j} k(y_i, y_j) - 2 \sum_{i,j} k(x_i, y_j)$ ^v	all-pairs	non-zero-sum game ^{vi}

ⁱ We show the empirical form of the loss in the function space. Rigorously speaking, the provided form is the the loss for one mini-batch; in practice, in different iterations of SGD we will use different samples of x_i, y_j . For the empirical loss in the parameter space, we shall replace f by f_θ and y_j by $G_w(z_j)$. ⁱⁱ Besides the zero-sum game form (min-max form), RpGAN can be easily modified to a non-zero-sum game form ("non-saturating version" proposed in [35]).

ⁱⁱⁱ The precise expression of RaGAN (relativistic averaging GAN) shall be $\sum_j h_1(\frac{1}{n} \sum_{i=1}^n f_\theta(x_i) - f_\theta(y_j)) + \sum_i h_2(\frac{1}{n} \sum_{j=1}^n f_\theta(y_j) - f_\theta(x_i))$, but for simplicity we only present one term in the table.

^{iv} Here $f(X)_{(1)} \leq \dots \leq f(X)_{(n)}$ and $f(Y)_{(1)} \leq \dots \leq f(Y)_{(n)}$ are the sorted versions of $f(x_i)$'s and $f(y_i)$'s respectively.

^v Here k is the Coulomb kernel, defined as $k(u, v) = \frac{1}{(\sqrt{\|u-v\|^2 + \epsilon^2})^\alpha}$ where $u, v \in \mathbb{R}^d, \alpha \leq d-2$ and $\epsilon > 0$. The original

form of Coulomb-GAN is a non-zero-sum game, but it is straightforward to transfer the formulation to a pure minimization form since the discriminator-minimization problem has a closed form solution (used in the proof of [83, Theorem 2]). We presented the transformed minimization problem here. ^{vi} Coulomb-GAN is presented as a non-zero-sum game, but as mentioned earlier it can be transformed to a minimization problem. The original Coulomb-GAN uses a smoothing operator in the generator loss; in this empirical form, we omit the smoothing operator for easier comparison (thus it is not the same as Coulomb-GAN). In the table, we show the resulting loss in the pure minimization form. Unlike SepGAN and RpGAN that can be written as either min-max form or non-zero-sum game form, we point out that there is no min-max form for Coulomb-GAN, since the design principle of Coulomb-GAN is very different from typical GANs.

Coulomb-GAN. Unterthiner et al. [83] argued that mode collapse can be a local Nash equilibrium in an example of two clusters (see [83, Appendix A.1]). They further proposed ColumbGAN and claimed that every local Nash equilibrium is a global Nash equilibrium (see [83, Theorem 2]). Their study is different from ours in a few aspects. **First**, they still consider the pdf p_g , though restrict the possible movement of p_g (according to a continuity equation). In contrast, we consider the empirical loss in particle space. **Second**, the bad landscape of JS-GAN is discussed in words for the 2-cluster case [83, Appendix A.1], but not formally proved. In contrast, we prove rigorous result for the general case. **Third**, they do not study parameter space (though with informal discussion). **Fourth**, they do not present landscape-related experiments, such as the narrow-net experiments we have done.

Common idea: Coupling true data and fake data. Interestingly, similar to IMLE and RpGAN, ColumbGAN also coupled the true data and fake data in the loss functions. RpGAN, RaGAN (a variant of RpGAN considered in [41]), IMLE and ColumbGAN differ in two aspects: the specific form of coupling (pairing, comparing with average, comparing with the closest, all possible pairs), and the specific form of optimization (pure minimization, min-max, non-zero-sum game). See the comparison in Table 3. It is interesting that all three lines of work choose to couple true data and fake data to resolve the issue of mode collapse. We suspect it is hard to prove similar results on the landscape of empirical loss for IMLE and Coulomb-GAN.

Relation to (max-)sliced Wasserstein GAN. We point out that the sliced Wasserstein GAN (sliced-WGAN) [24] and the max-sliced Wasserstein GAN (max-sliced-WGAN) [25] also couple the true data and fake data. For any function f , denote $f(X) = (f(x_1), \dots, f(x_n))$ and $f(Y) = (f(y_1), \dots, f(y_n))$. The empirical version of the max-sliced Wasserstein GAN can be written as

$$\min_Y \max_{|f|_L \leq 1} W_2(f(X), f(Y))^2. \quad (10)$$

Here f is a neural net with codomain \mathbb{R} , and W_2 is the Wasserstein-2-distance. Denote $f(X)_{(1)} \leq \dots \leq f(X)_{(n)}$ and $f(Y)_{(1)} \leq \dots \leq f(Y)_{(n)}$ as the sorted versions of $f(x_i)$'s and $f(y_i)$'s respec-

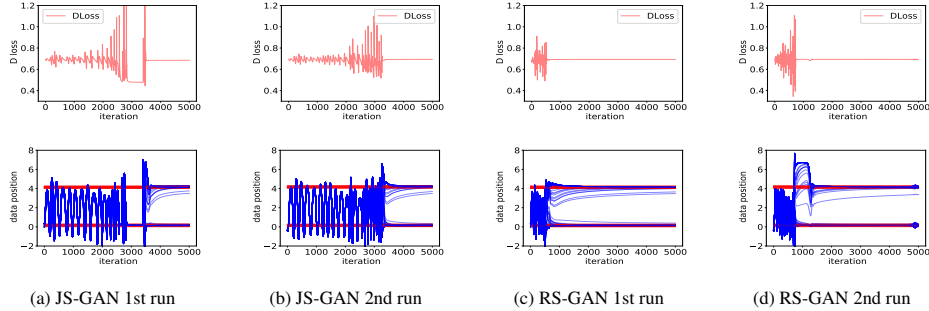


Figure 7: Comparison of JS-GAN and RS-GAN for two different runs. First row: D loss; second row: fake data movement during training.

tively. Then Eq. (10) is equivalent to

$$(\text{max-})\text{sliced-WGAN}^5 : \min_Y \max_{|f|_L \leq 1} \sum_{i=1}^n [f(X)_{(i)} - f(Y)_{(i)}]^2. \quad (11)$$

This form is quite close to RpGAN (when $h(t) = t^2$): the only differences are the sorting of $f(X)$, $f(Y)$ and the extra constraint $|f|_L \leq 1$. The extra constraint $|f|_L \leq 1$ is due to unbounded h , and can be removed if we use an upper bounded h (which leads to a sorting version of RpGAN). See the comparison of max-sliced-WGAN with RpGAN and other models in Table 3.

Nash equilibria for Gaussian data. A very recent work Farnia and Ozdaglar [28] shows that for a non-realizable case (with a linear generator) Nash equilibria may not exist for learning a Gaussian distribution. This setting is quite different from ours.

B 2-Cluster Experiments: Details and More Discussions

In this part, we present details of the experiments in Section 5 and other complementary experiments.

Experimental Setting. The code is provided in “GAN_2Cluster.py”. We sample 100 points from two clusters of data near 0 and 4 (roughly 50 in each cluster). We use GD with momentum parameter 0.9 for both D and G . The default learning rate is $(\text{Dlr}, \text{Glr}) = (10^{-2}, 10^{-2})$. The default inner-iteration-number for the discriminator and the generator are $(\text{DIter}, \text{GIter}) = (10, 10)$. The discriminator and generator net are a 4-layer network (with 2 hidden layers) with sigmoid activation and tanh activation respectively. The default neural network width $(\text{Dwidth}, \text{Gwidth}) = (10, 5)$. We will also discuss the results of other hyperparameters. The default number of training iterations is $\text{MaxIter} = 5000$. We use the non-saturating versions for both JS-GAN and RS-GAN.

Understanding the effect of mode collapse, by checking D loss evolution and data movement.

In the main text, we discussed that mode collapse can slow down training of JS-GAN. For easier understanding of the training process, we add the visualization of the data movement (which is possible since we are dealing with 1-dimensional data) in Figure 7. We use the y-axis to denote the data position, and x-axis to denote the iteration. The blue curves represent the movement of all fake data during training, and the red straight lines represent the position of true data (two clusters). The training time may vary across different runs, but overall the time for JS-GAN is about 2-4 times longer than that for RS-GAN.

Effect of width. The default width is $(\text{Dwidth}, \text{Gwidth}) = (10, 5)$. We tested two other settings: $(20, 10)$ and $(5, 3)$. For the wide-network setting, the convergence of both JS-GAN and RS-GAN are much faster, but RS-GAN is still faster than JS-GAN in most cases; see Fig. 8. For the narrow-network setting, RS-GAN can recover two modes in all five runs, while JS-GAN fails in two of the five runs (within 5k iterations). See Fig. 9 for one success case of JS-GAN and one failure case of JS-GAN. In the failure case, JS-GAN completely gets stuck at mode collapse, and the D loss is stuck at around 0.48, consistent with our theory.

⁵Note that max-sliced-WGAN in Deshpande et al. [25] uses $\min_Y \max_{\|v\| \leq 1, |g|_L \leq 1} W_2(v^T g(X), v^T g(Y))^2$, while sliced-WGAN in Deshpande et al. [24] uses $\min_Y \mathbb{E}_{\|v\|=1} \max_{|g|_L \leq 1} W_2(v^T g(X), v^T g(Y))^2$. In Eq. (10) we use $f(u)$ to replace $v^T g(u)$ to simplify the expression; although technically, f and $v^T g$ are not equivalent, this minor difference does not affect our discussion.

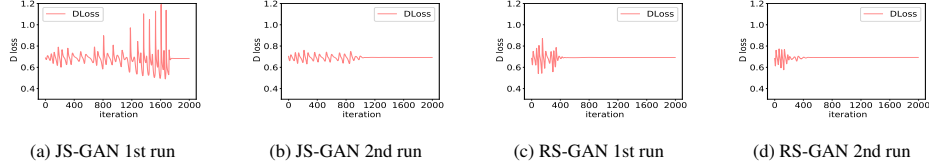


Figure 8: Wide network (Dwidth, Gwidth) = (20, 10): JS-GAN and RS-GAN in two different runs. Compare to regular widths (Dwidth, Gwidth) = (10, 5), both GANs converge faster. Anyhow, RS-GAN is still 2-3 times faster than JS-GAN.

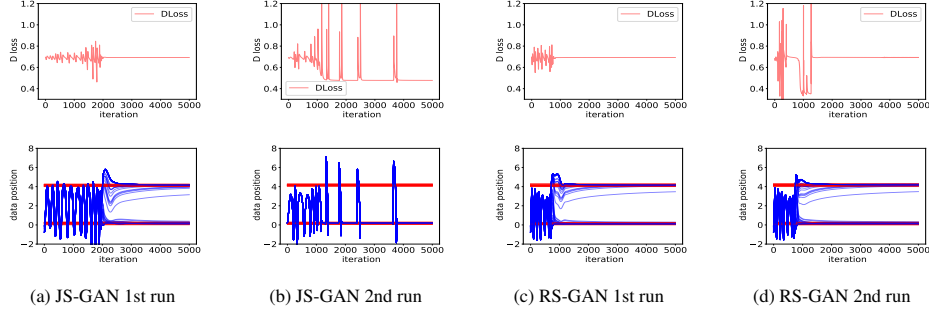


Figure 9: Narrow network setting: Comparison of JS-GAN and RS-GAN in two runs. RS-GAN is a few times faster than JS-GAN in general. Compare to default widths (D width 10, G width 5), both GANs converge slower. In one case (b), JS-GAN gets stuck at mode collapse.

Other hyperparameters. Besides the width, the learning rates and (Dlter, Glter) will also affect the training process. As for (Dlter, Glter), we use (10, 10) as default, but other choices such as (5, 2) and (1, 1) also work. As for learning rates, we use (0.01, 0.01) as default, but smaller learning rates such as (0.001, 0.001) also work. Different from the default hyper-parameters, for some hyper-parameters, the D loss of JS-GAN does not reach 0.48, indicating that the basin only attracts the iterates half-way. Nevertheless, in most settings RS-GAN is still faster than JS-GAN.

C Result and Experiments for Imbalanced Data Distribution

In the main results, we assume x_i 's are distinct. In this section, we allow x_i 's to be in general positions, i.e., they can overlap. The 2-point model can only approximate two balanced clusters. Allowing x_i 's to overlap, we are able to analyze imbalanced two clusters. We will show: (i) a theoretical result for 2-cluster data; (ii) experiments on imbalanced 2-cluster data and MNIST.

C.1 Imbalanced Data: Math Results for Two-Clusters

Assume there are n true data points $X = (x_1, \dots, x_n)$ in two modes with proportion α and $1 - \alpha$ respectively, where $\alpha > 0.5$. More precisely, assume $x_1 = x_2 = \dots = x_{n\alpha}$ and $x_{n\alpha+1} = \dots = x_n$, and denote two multi-sets $\mathcal{X}_1 = \{x_1, x_2, \dots, x_{n\alpha}\}$ and $\mathcal{X}_2 = \{x_{n\alpha+1}, x_2, \dots, x_n\}$. Denote $Y = (y_1, \dots, y_n)$ as the tuple of all generated points, and let \mathcal{Y} be the multiset $\{y_1, \dots, y_n\}$.

Claim C.1. Consider the JS-GAN loss defined in Eq. (1), where X is defined above. We have

$$\begin{aligned} \phi_{\text{JS}}(Y, X) &= q_\alpha(m_1) + q_{1-\alpha}(m_2), \text{ if } |\mathcal{X}_1 \cap \mathcal{Y}| = m_1, |\mathcal{X}_2 \cap \mathcal{Y}| = m_2, \\ \text{where } q_\alpha(m) &\triangleq \frac{\alpha}{2} \log(\alpha n) + \frac{m}{2n} \log m - \frac{\alpha n + m}{2n} \log(\alpha n + m). \end{aligned} \quad (12)$$

As a result, the global minimal loss is $-\log 2$, which is achieved iff $\mathcal{Y} = \mathcal{X}_1 \cup \mathcal{X}_2$.

Corollary C.1. Suppose $\hat{Y} = (\hat{y}_1, \dots, \hat{y}_n)$ satisfies $|\mathcal{X}_1 \cap \hat{\mathcal{Y}}| = n_1, |\mathcal{X}_2 \cap \hat{\mathcal{Y}}| = n - n_1$, where $\hat{\mathcal{Y}} = \{\hat{y}_1, \dots, \hat{y}_n\}$ is the multiset of all \hat{y}_j 's, then \hat{Y} is a strict local minimum. Moreover, if $n_1 \neq n\alpha$, then \hat{Y} is a sub-optimal strict local minimum.

The proofs of Claim C.1 and Corollary C.1 are given in Appendix H.3.

Denote $m_1 \triangleq |\mathcal{X}_2 \cap \mathcal{Y}|, m_2 \triangleq |\mathcal{X}_1 \cap \mathcal{Y}|$. The value $q_\alpha(n)$ indicates the value of $\phi(Y, X)$ at the mode collapsed pattern (state 1a) where $m_1 = n, m_2 = 0$. Note that $q_\alpha(n) = \frac{\alpha}{2} \log \frac{\alpha}{\alpha+1} + \frac{1}{2} \log \frac{1}{\alpha+1}$ is a strictly decreasing function of α . When $\alpha = 1/2$, $q_\alpha(n) = \frac{1}{4} \log \frac{1}{3} + \frac{1}{2} \log \frac{2}{3} \approx -0.4774$; when $\alpha = 2/3$, $q_\alpha(n) \approx -0.5608$. The more imbalanced the data are (larger α), the smaller $q_\alpha(n)$, and

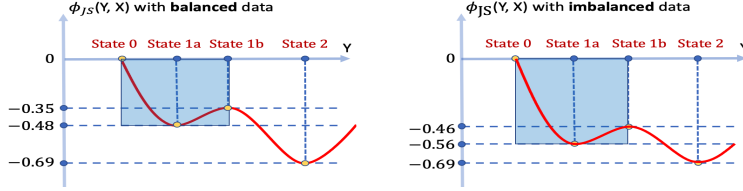


Figure 10: Illustration of the landscape of JS-GAN for balanced two clusters with $\alpha = 0.5$ (left) and imbalanced two clusters with $\alpha = 2/3$ (right). Denote $m_i \triangleq |\mathcal{X}_i \cap \mathcal{Y}|$, $i = 1, 2$. Here state 0, state 1a, state 1b, state 2 represent $(m_1, m_2) = (0, 0), (n\alpha, 0), (n\alpha, 0), (n\alpha, n(1 - \alpha))$ respectively. By Claim C.1, for $\alpha = 1/2$, $q_\alpha(n) \approx -0.48$ and $q_\alpha(\alpha n) \approx -0.35$; for $\alpha = 2/3$, $q_\alpha(n) \approx -0.56$ and $q_\alpha(\alpha n) \approx -0.46$. Different from the 2-point-case landscape in Fig. 5, there should be some intermediate patterns (satisfying $m_1 \leq n, m_2 = 0$), but for simplicity we do not show them. From state 1a to state 2, \mathcal{Y} can go through state 1b or go through state 0, but we only show the path through state 1b. We view the gap between state 0 and state 1a as an approximation of the “depth” of the basin.

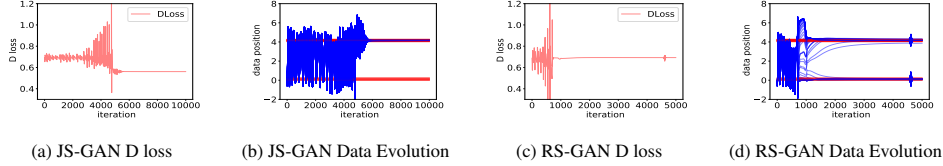


Figure 11: Imbalanced 2-cluster result: comparison of JS-GAN in (a) and (b), and RS-GAN in (c) and (d). (a) and (c): evolution of D loss; (b) and (d): data position movement during training.

further the deeper the basin. In Figure 10, we compare the loss landscape of the balanced case $\alpha = 1/2$ and the imbalanced case $\alpha = 2/3$.

We suspect that the deeper basin in the imbalanced case will make it harder to escape mode collapse for JS-GAN. We then make the following prediction: for JS-GAN, mode collapse is a more severe issue for imbalanced data than it is for balanced data. For RS-GAN, the performance does not change much as data becomes more imbalanced. We will verify this prediction in the next subsections.

C.2 Experiments

2-Cluster Experiments. For the balanced case, the experiment is described in Appendix B. Both JS-GAN and RS-GAN can converge to the two-mode-distribution. For the imbalanced case where $\alpha = \frac{2}{3}$, with other hyper-parameters unchanged, JS-GAN falls into mode collapse while RS-GAN generates the true distribution (2/3 in mode 1 and 1/3 in mode 2) (see Fig. 11). The loss $\phi_{\text{JS}}(Y, X)$ ends up at approximately -0.56, which matches Claim C.1.

MNIST experiments. To ease visualization, we create an MNIST sub-dataset only containing 5’s and 7’s. We use the CNN structure of Tab. 7 and train for $30k$ iterations. For the balanced case, the number of 5’s and 7’s are identical (i.e., ratio 1:1). Both JS-GAN and RS-GAN generate a roughly equal number of 5’s and 7’s, as shown in Fig. 12(a,b). For the imbalanced case with 4 times more 7’s than 5’s (ratio 1:5), JS-GAN only generates 7’s, while RS-GAN generates 13 5’s among 64 generated samples, aligning with the true data distribution (see Fig. 12(c,d)).

The above two experiments verify our earlier prediction that RS-GAN is robust to imbalanced data while JS-GAN easily gets stuck at mode collapse for imbalanced data.

D Experiments of Bad Initialization

A bad optimization landscape does not mean the algorithm always converges to bad local minima⁶. A ‘bad’ landscape means is that there exists a “bad” initial point (the blue point in Fig. 13(a)) that it will lead to a ‘bad’ final solution upon training. In contrast, a good landscape is more robust to the initial point: starting from any initial point (e.g., two points shown in Fig. 13(b)), the algorithm can still find a good solution. Therefore, bad optimization landscape of JS-GAN does not mean the performance of JS-GAN is bad for *any* initial point, but it should imply that JS-GAN is bad for *certain* initial points.

Next, we will show experiments that support this prediction.

⁶Technically since we are not dealing with a pure minimization problem, we should say “the algorithm converges to a bad attractor”. But for simplicity of illustration, we still call it “local minimum.”

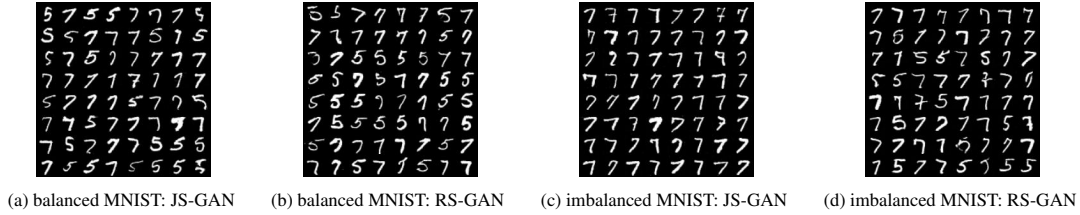


Figure 12: Balanced and Imbalanced MNIST setting: Comparison of JS-GAN and RS-GAN.

5-Gaussian Experiments. We consider a 2-dimensional 5-Gaussian distribution as illustrated in Fig. 14(a). We design a procedure to find an initial discriminator and generator. For JS-GAN or RS-GAN, in some runs we obtain mode collapse and in some runs we obtain perfect recovery. Firstly, for the runs achieving perfect recovery (Fig. 14(b)) in JS-GAN and RS-GAN respectively, we pick the generators at the converged solution, which we denote as G_{JS0} and G_{RS0} respectively. Secondly, for the runs attaining mode collapse (Fig. 14(c)) in JS-GAN and RS-GAN respectively, we pick the discriminators at the converged solution, referred to as D_{JS0} and D_{RS0} . Then we re-train both JS-GAN and RS-GAN from (D_{JS0}, G_{JS0}) and (D_{RS0}, G_{RS0}) respectively.

We define an evaluation metric $\Psi = \sum_{k=1}^K \min_{1 \leq i \leq 10^4} (\alpha \|x_i - C_k\|)$, where C_k 's are the cluster centers, α is a scalar and x_i 's are 10^4 true data samples. We repeat the experiment $S = 50$ times and compute the average Ψ . The larger the metric, the worse the generated points. As shown in Fig. 14(a), the metric Ψ is much higher for JS-GAN than for RS-GAN, for various learning rates lr .

JS-GAN	65	78	60	93	139	137
RS-GAN	29	30	30	26	32	56
	$5e-07$	$1e-06$	$5e-06$	$1e-05$	$5e-05$	$1e-04$

generator lr = discriminator lr

Figure 15: MNIST experiment

MNIST Experiments. We use a similar strategy to find initial parameters for MNIST data. Fig. 15 (also in Sec. 6) shows that RS-GAN generates much lower FID scores (30+ gap) than JS-GAN.

The two experiments verify our prediction that RS-GAN is more robust to initialization, which supports our theory that RS-GAN enjoys a better landscape than JS-GAN.

E Experiments of Regular Training: More Details and More Results

In this section, we present details of the regular experiments in Sec. 6 and a few more experiments.

E.1 Experiment Details and More Experiments with Logistic Loss

Non-saturating version. Following the standard practice [35], if $\lim_{t \rightarrow \infty} h(t) = 0$, we use the non-saturating version of RpGAN in practical training:

$$\begin{aligned} \min_{\theta} L_D(\theta; w) &\triangleq \frac{1}{n} \sum_i h(f_{\theta}(x_i) - f_{\theta}(G_w(z_i))), \\ \min_w L_G(w; \theta) &\triangleq \frac{1}{n} \sum_i h(f_{\theta}(G_w(z_i)) - f_{\theta}(x_i)). \end{aligned} \quad (13)$$

For logistic and hinge loss, we use Eq. (13). For least-square loss, we use the original min-max version (check Appendix E.3 for more). We use alternating stochastic GDA to solve this problem.

Neural-net structures: We conduct experiments on two datasets: CIFAR-10 (32×32 size) and STL-10 (48×48 size) on both standard CNN and ResNet. As mentioned in Sec. 6, we also conduct experiments on the narrower nets: we reduce the number of channels for all convolutional layers in the generator and discriminator to (1) half, (2) quarter and (3) bottleneck (for ResNet structure), The

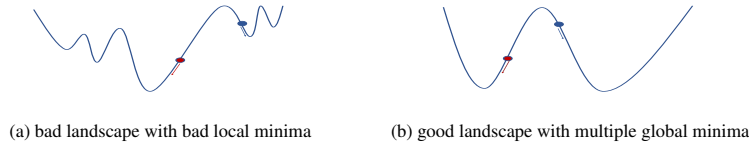


Figure 13: Left: for a bad landscape, a good initial point (red) leads to convergence to a global optima while a bad one (blue) does not. Right: for a good landscape, two initial points both converge to global minima.

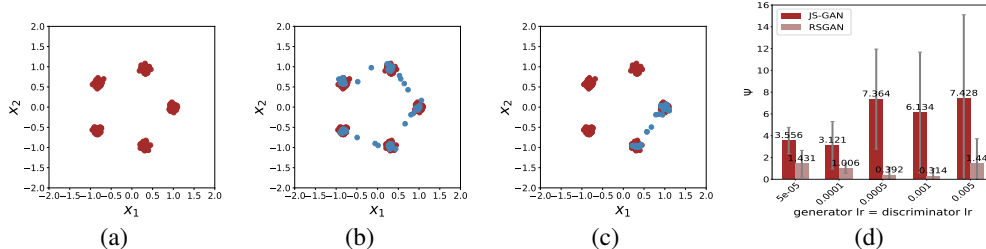


Figure 14: Five Gaussian experiment. (a): ground truth. (b): generated data covers all five clusters. (c): mode collapse happens and only two clusters get covered. (d) JS-GAN and RSGAN’s loss Ψ under different lr (generator lr = discriminator lr).

	CIFAR-10		CIFAR-10+EMA		STL-10+EMA	
	IS \uparrow	FID \downarrow	IS \uparrow	FID \downarrow	IS \uparrow	FID \downarrow
ResNet						
JS-GAN+SN	8.03 \pm 0.10	20.06 \pm 0.18	8.41 \pm 0.09	17.79 \pm 0.43	9.14 \pm 0.12	33.06
RS-GAN+SN	7.94 \pm 0.09	19.79 \pm 0.57	8.37 \pm 0.10	17.75 \pm 0.56	9.23 \pm 0.08	31.87
JS-GAN+SN+GD channel/2	7.77 \pm 0.08	23.36 \pm 0.46	8.24 \pm 0.08	20.55 \pm 0.59	8.69 \pm 0.08	42.05
RS-GAN+SN+GD channel/2	7.76 \pm 0.07	21.63 \pm 0.51	8.21 \pm 0.09	18.91 \pm 0.45	8.77 \pm 0.13	39.31
JS-GAN+SN+GD channel/4	6.75 \pm 0.06	44.39 \pm 4.38	7.18 \pm 0.06	38.75 \pm 6.28	8.42 \pm 0.06	52.38
RS-GAN+SN+GD feature/4	7.20 \pm 0.07	31.40 \pm 0.78	7.60 \pm 0.06	26.85 \pm 0.56	8.43 \pm 0.10	48.92
JS-GAN+SN+BottleNeck	7.51 \pm 0.07	27.33 \pm 1.05	7.99 \pm 0.10	23.71 \pm 0.86	8.37 \pm 0.08	47.97
RS-GAN+SN+BottleNeck	7.52 \pm 0.10	25.05 \pm 0.35	8.06 \pm 0.11	21.29 \pm 0.22	8.48 \pm 0.06	44.60

Table 4: Repeat the experiments (logistic loss) in Tab. 2 with at least three seeds.

architectures are shown in Tab. 7 (CNN), Tab. 9 (ResNet for CIFAR) and Tab. 10 (ResNet for STL) and Tab. 11 (Bottleneck for CIFAR) and Tab. 12 (Bottleneck for STL).

Hyper-parameters: We use a batchsize of 64. For CIFAR-10 on ResNet we set $\beta_1 = 0$ and $\beta_2 = 0.9$ in Adam. For others, $\beta_1 = 0.5$ and $\beta_2 = 0.999$. We use $GIter = 1$ for both CNN and ResNet. We also use $DIter = 1$ for CNN and $DIter = 5$ for ResNet. We fix the learning rate for the discriminator (dlr) to be $2e-4$. For RpGANs, we find that the learning rate for the generator (glr) needs to be larger than dlr to keep the training balanced. Thus we tune glr using parameters in the set $2e-4, 5e-4, 1e-3, 1.5e-3$. For SepGAN, we set $glr = 0.0002$ for SepGANs (JS-GAN, hinge-GAN) as suggested by [67, 76]⁷. See Tab. 13 for the learning rate of RS-GAN and hyper-parameters of WGAN-GP.

More details of EMA: In Sec. 6, we conjectured that the effect of EMA (exponential moving average) [88] and RpGAN are additive. Suppose $w^{(t)}$ is the generator parameter in t -th iteration of one run, the EMA generator at the t th iteration is computed as follows $w_{EMA}^{(t)} = \beta w_{EMA}^{(t-1)} + (1-\beta)w^{(t)}$, where $w_{EMA}^{(0)} = w^{(0)}$. Note that EMA is a post-hoc processing step, and does not affect the training process. Intuitively, the EMA generator is closer to the bottom of a basin while the real training is circling around a basin due to the minmax structure. We set $\beta = 0.9999$. As Tab. 4 shows, while EMA improves both JS-GAN and RS-GAN, RS-GAN is still better than JS-GAN.

Results on Logistic Loss with More Seeds: Besides the result in Tab. 2, we run at least 3 extra seeds for all experiments with ResNet structure on CIFAR-10 to show that the results are consistent across different runs. We report the results in Tab. 4, and find RS-GAN is still better than JS-GAN and the gap increases as the networks become narrower.

Samples of image generation: Generated samples obtained upon training on CIFAR-10 are given in Fig. 16 for CNN, Fig. 17 for ResNet. Generated samples obtained upon training on STL-10 dataset are given in Fig. 18 for CNN, Fig. 19 for ResNet. Instead of cherry-picking, all sample images are generated from random sampled Gaussian noise.

⁷We tuned glr in the set $2e-4, 5e-4, 1e-3, 1.5e-3$ and find that $glr = 2e-4$ performs the best in most cases for SepGAN, so we follow the suggestion of [67, 76].

	CIFAR-10			CIFAR-10 + EMA		
	IS \uparrow	FID \downarrow	FID Gap	IS \uparrow	FID \downarrow	FID Gap
ResNet + Hinge Loss						
Hinge-GAN	7.92 \pm 0.08	21.30		8.44 \pm 0.10	17.43	
Hinge-GAN +GD channel/2	7.63 \pm 0.05	27.21		7.90 \pm 0.08	24.35	
Hinge-GAN +GD channel/4	6.79 \pm 0.09	37.51		7.39 \pm 0.07	34.45	
Hinge-GAN +BottleNeck	7.16 \pm 0.10	33.24		7.91 \pm 0.09	26.56	
Rp-Hinge-GAN						
Rp-Hinge-GAN	7.84 \pm 0.09	19.10	2.20	8.21 \pm 0.09	17.19	0.24
Rp-Hinge-GAN +GD channel/2	7.77 \pm 0.08	21.10	6.11	8.34 \pm 0.11	19.19	5.17
Rp-Hinge-GAN +GD channel/4	7.21 \pm 0.11	29.41	8.10	7.77 \pm 0.08	25.57	8.88
Rp-Hinge-GAN +BottleNeck	7.52 \pm 0.07	23.28	9.96	8.05 \pm 0.07	22.03	4.53

Table 5: Comparison of Hinge-GAN and Rp-Hinge-GAN. We also show the FID gap between Rp-Hinge-GAN with Hinge-GAN (e.g. 2.20 = 21.30 – 19.10 and 9.96 = 33.24 – 23.28).

E.2 Experiments with Hinge Loss

Hinge loss has become popular in GANs [82, 67, 18]. The empirical loss of hinge-GAN is

$$\min_{\theta} L_D^{\text{Hinge}}(\theta; w) \triangleq \frac{1}{2n} \left[\sum_i \max(0, 1 - D_{\theta}(x_i)) + \sum_i \max(0, 1 + D_{\theta}(G_w(z_i))) \right],$$

$$\min_w L_G^{\text{Hinge}}(w; \theta) \triangleq -\frac{1}{n} \sum_i D_{\theta}(G_w(z_i)).$$

Note that Hinge-GAN applies the hinge loss for the discriminator, and linear loss for the generator. This is a variant of SepGAN with $h_1(t) = h_2(t) = -\max(0, 1 - t)$.

The Rp-hinge-GAN is RpGAN given in Eq. (13) with $h(t) = -\max(0, 1 - t)$:

$$\min_{\theta} L_D^{\text{R-Hinge}}(\theta; w) \triangleq \frac{1}{n} \sum_i \max(0, 1 + (f_{\theta}(G_w(z_i)) - f_{\theta}(x_i))),$$

$$\min_w L_G^{\text{R-Hinge}}(w; \theta) \triangleq \frac{1}{n} \sum_i \max(0, 1 + (f_{\theta}(x_i) - f_{\theta}(G_w(z_i)))).$$

We compare them on ResNet with the hyper-parameter settings in Appendix E.1. As Tab. 5 shows, Rp-Hinge-GAN (both versions) performs better than Hinge-GAN. For narrower networks, the gap is 4 to 9 FID scores, larger than the gap for the logistic loss.

E.3 Experiments with Least Square Loss

We consider the least square loss. The LS-GAN [62] is defined as follows:

$$\min_{\theta} L_D^{\text{LS}}(\theta; w) \triangleq \frac{1}{2n} \left[\sum_i (f_{\theta}(x_i) - 1)^2 + \sum_i f_{\theta}(G_w(z_i))^2 \right],$$

$$\min_w L_G^{\text{LS}}(w; \theta) \triangleq \frac{1}{n} \sum_i (f_{\theta}(G_w(z_i)) - 1)^2.$$

This is a non-zero-sum variant of SepGAN with $h_1(t) = -(1 - t)^2$, $h_2(t) = -t^2$.

Rp-LS-GAN addresses the following objectives:

$$\min_{\theta} L_D^{\text{Rp-LS}}(\theta; w) \triangleq \frac{1}{n} \sum_i (f_{\theta}(x_i) - f_{\theta}(G_w(z_i)) - 1)^2,$$

$$\min_w L_G^{\text{Rp-LS}}(w; \theta) \triangleq -L_D^{\text{Rp-LS}}(\theta; w) = -\frac{1}{n} \sum_i (f_{\theta}(x_i) - f_{\theta}(G_w(z_i)) - 1)^2. \quad (14)$$

For least square loss $h(t) = -(t - 1)^2$, the gradient vanishing issue due to h does not exist, thus we can use the min-max version given in Eq. (14) in practice. Our version of Rp-LS-GAN is actually different from the version of Rp-LS-GAN in [41] which is similar to Eq. (13) with least square h .

In Tab. 6 we compare LS-GAN and Rp-LS-GAN on CIFAR-10 with CNN architectures detailed in Tab. 7. As Tab. 6 shows, Rp-LS-GAN is slightly worse than LS-GAN in regular width, but is better than LS-GAN (with 5.7 FID gap) when using 1/4 width.

F Experiments on High Resolution Data

There are two approaches to achieve a good landscape: one uses a wide enough neural net [73, 50], and the other uses a large enough number of samples (approaching convexity of pdf space). As we

	Regular width			channel/2			channel/4		
	IS	FID	FID Gap	IS	FID	FID Gap	IS	FID	FID Gap
LS-GAN	6.91±0.10	32.93		6.63±0.08	37.83		5.69±0.10	48.63	
Rp-LS-GAN	7.09±0.07	34.78	-1.85	6.94±0.04	34.34	3.49	6.22±0.10	42.86	5.77

Table 6: Comparison of LS-GAN and Rp-LS-GAN on CIFAR-10 with the CNN structure.

discuss in Sec. 2 (see also Appendix G.1), when the number of samples is far from enough for filling the data space, the convexity (of pdf space) may vanish. A higher dimension of data implies a larger gap between empirical loss and population loss, thus the non-convexity issue will become more severe. Thus we conjecture that JS-GAN suffers more for higher resolution data generation.

We consider 256×256 LSUN Church and Tower datasets with CNN architecture in Tab. 8. For RS-GAN, we set $\text{glr} = 1e-3$ and $\text{dlr} = 2e-4$. We train 100,000 iterations with batchsize 64. The generated images are presented in Fig. 20. For both datasets, RS-GAN outperforms JS-GAN visually.

G Discussions on Empirical Loss and Population Loss (complements Sec. 2)

As mentioned in Sec. 2, the pdf space view (the population loss) was first used in [35], and became quite popular for GAN analysis. See, e.g., [71, 40, 20]. In this part, we provide more discussions on the relation of empirical loss and population loss in GANs.

G.1 Particle space or probability space?

Suppose $p_z = \mathcal{N}(0, I_{d_z})$ (or other distributions) is the distribution of the latent variable z , and $Z = (z_1, \dots, z_n)$ are the samples of latent variables. During training, the parameter w of the generator net G_w is moving, and, as a result, both the pdf $p_g = G_w(p_z)$ and the particles $y_j = G_w(z_j)$ move accordingly. Therefore, GAN training can be viewed as either probability space optimization or particle space optimization. The two views (pdf space and particle space) are illustrated in Figure 1.

In the probability space view, an implicit assumption is that the pdf p_g moves *freely*; in the particle space view, we assume the particles move *freely*. Free-particle-movement implies free-pdf-movement if the particles almost occupy the whole space (a one-mode distribution), as shown in Fig. 21. However, for multi-mode distributions in high-dimensional space, the particles are sparse in the space, and free-particle-movement does NOT imply free-pdf-movement. This gap was also pointed out in [83]; here, we stress that the gap becomes larger for sparser samples (either due to few samples or high dimension). This forms the foundation for experiments in App. F.

To illustrate the gap between free-pdf-movement and free-particle-movement, we use an example of learning a two-mode distribution p_{data} . Suppose we start from an initial two-mode distribution p_g , as shown Figure 22. To learn p_{data} , we need to do two things: first, move the two modes of p_g to roughly overlap with the two modes of p_{data} which we call “macro-learning”; second, adjust the distributions of each mode to match those of p_{data} , which we call “micro-learning.” This decomposition is illustrated in Fig. 22 and 23. In micro-learning, the pdf can move freely, but in macro-learning, the whole mode has to move together and cannot move freely in the pdf space.

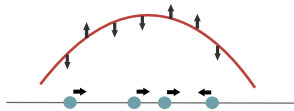


Figure 21: Illustration of the learning process of the single mode. The generated samples are moving, which corresponds to adjustment of the probability densities.

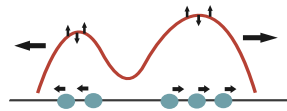


Figure 22: Illustration of the process of learning a multi-mode distribution. We decompose this process into two parts in the next figure.

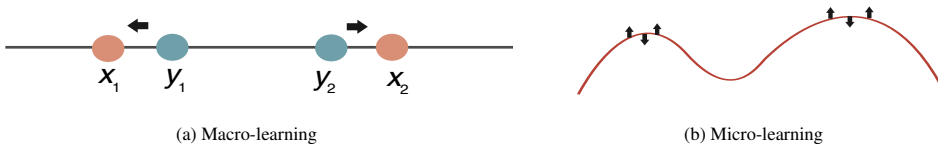


Figure 23: Decomposing learning a multi-mode distribution into macro-learning and micro-learning. Macro-learning refers to the movement of the whole mode towards the underlying data mode. Micro-learning refers to the adjustment of the distribution within each mode. If macro-learning fails, then an entire mode is missed in the generated distributions, which corresponds to mode collapse.

G.2 Empirical loss and population loss

The population version of RpGAN [41] is $\min_{p_{\text{data}}} \phi_{\text{R,E}}(p_g, p_{\text{data}})$, where

$$\phi_{\text{R,E}}(p_g, p_{\text{data}}) = \sup_{f \in C(\mathbb{R}^d)} \mathbb{E}_{(x,y) \sim (p_g, p_{\text{data}})} [h(f(x) - f(y))]. \quad (15)$$

Suppose we sample $x_1, \dots, x_n \sim p_{\text{data}}$ and $y_1, \dots, y_n \sim p_g$, then $\frac{1}{n} \sum_{i=1}^n [h(f(x_i) - f(y_i))]$ is an approximation of $\mathbb{E}_{(x,y) \sim (p_g, p_{\text{data}})} [h(f(x) - f(y))]$. The empirical version of RpGAN addresses $\min_{Y \in \mathbb{R}^d \times n} \phi_{\text{R}}(Y, X)$, where

$$\phi_{\text{R}}(Y, X) = \sup_{f \in C(\mathbb{R}^d)} \frac{1}{n} \sum_{i=1}^n [h(f(x_i) - f(y_i))]. \quad (16)$$

Our analysis is about the geometry of $\phi_{\text{R}}(Y, X)$ in Eq. (16). In practical SGDA (stochastic GDA), at each iteration we draw a mini-batch of samples and update the parameters based on the mini-batch. The samples of true data x_i are re-used multiple times (similar to SGD for a finite-sum optimization), but the samples of latent variables z_i are fresh (similar to on-line optimization). Due to the re-use of true data, stochastic GDA shall be viewed as an online optimization algorithm for solving Eq. (16) where x_i 's can be the same. Recall that in the main results, we have assumed that x_i 's are distinct, thus there is a gap between our results and practice. Extending our results to the case of non-distinct x_i 's requires extra work. This was done in Claim C.1 for the 2-cluster setting. But for readability we do not further study this setting in the more general cases. We leave this to future work.

G.3 Generalization and overfitting of GAN

One may wonder whether fitting the empirical distribution can cause memorization and failure to generate new data. Arora et al. [5] proved that for many GANs (including JS-GAN) with neural nets, only a polynomial number of samples are needed to achieve a small generalization error. We suspect that a similar generalization bound can be derived for RpGAN.

We provide some intuition why fitting the empirical data distribution via a GAN may avoid overfitting. Consider learning a two-cluster distribution as shown in Fig. 24. During training, we learn a generator that maps the latent samples z_i to x_i , thus fitting the empirical distribution. If we sample a new latent sample z_j , then the generator will map z_j to a new point x_j in the underlying data distribution (due to the continuity of the generator function). Thus the continuity of the generator (or the restricted power of the generator) provides regularization for achieving generalization.

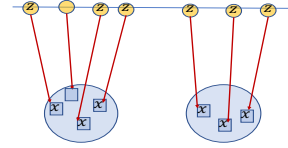


Figure 24: How to generate new point.

H Proofs for Section 3 (2-Point Case) and Appendix C (2-Cluster Case)

We now provide the proofs for the toy results (i.e., the case $n = 2$).

H.1 Proof of Claim 3.1 and Corollary 3.1 (for JS-GAN)

Proof of Claim 3.1: We will compute values of $\phi_{\text{JS}}(Y, X)$ for all Y . Recall D can be any continuous function with range $(0, 1)$. Recall that $\phi_{\text{JS}}(Y, X) = \sup_D \frac{1}{2n} [\sum_{i=1}^n \log(D(x_i)) + \sum_{i=1}^n \log(1 - D(y_i))]$. Consider four cases. Denote a multiset $\mathcal{Y} = \{y_1, y_2\}$, and let $m_i = |\mathcal{Y} \cap \{x_i\}|, i \in \{1, 2\}$.

Case 1 (state 1): $m_1 = m_2 = 1$. Then the objective is

$$\sup_D \frac{1}{2} \left[\frac{1}{2} \log(D(x_1)) + \frac{1}{2} \log(1 - D(x_1)) + \frac{1}{2} \log(D(x_2)) + \frac{1}{2} \log(1 - D(x_2)) \right].$$

The optimal value is $-\log 2$, which is achieved when $D(x_1) = D(x_2) = \frac{1}{2}$.

Case 2 (state 1a): $\{m_1, m_2\} = \{0, 1\}$. WLOG, assume $m_1 = 1, m_2 = 0$, and $y_1 = x_1, y_2 \notin \{x_1, x_2\}$. The objective becomes

$$\sup_D \frac{1}{2} \left[\frac{1}{2} \log(D(x_1)) + \frac{1}{2} \log(D(x_2)) + \frac{1}{2} \log(1 - D(x_1)) + \frac{1}{2} \log(1 - D(y_2)) \right].$$

The optimal value $-\log 2/2$ is achieved when $D(x_1) = 1/2$, $D(x_2) \rightarrow 1$ and $D(y_2) \rightarrow 0$.

Case 3 (state 1b): $\{m_1, m_2\} = \{0, 2\}$. WLOG, assume $y_1 = y_2 = x_1$. The objective becomes

$$\sup_D \frac{1}{2} \left[\frac{1}{2} \log(D(x_1)) + \log(1 - D(x_1)) + \frac{1}{2} \log(D(x_2)) \right].$$

The optimal value $\frac{1}{4} \log \frac{1}{3} + \frac{1}{2} \log \frac{2}{3} \approx -0.4774$ is achieved when $D(x_1) = 1/3$ and $D(x_2) \rightarrow 1$.

Case 4 (state 2): $m_1 = m_2 = 0$, i.e., $y_1, y_2 \notin \{x_1, x_2\}$. The objective is:

$$\sup_D \frac{1}{2} \left[\frac{1}{2} \log(D(x_1)) + \frac{1}{2} \log(D(x_2)) + \frac{1}{2} \log(1 - D(y_1)) + \frac{1}{2} \log(1 - D(y_2)) \right].$$

These terms are independent, thus each term can achieve its supreme $\log 1 = 0$. Then the optimal value 0 is achieved when $D(x_1) = D(x_2) \rightarrow 1$ and $D(y_1) = D(y_2) \rightarrow 0$.

Proof of Corollary 3.1: Suppose ϵ is the minimal non-zero distance between two points of x_1, x_2, y_1, y_2 . Consider a small perturbation of \bar{Y} as $Y = (\bar{y}_1 + \epsilon_1, \bar{y}_2 + \epsilon_2)$, where $|\epsilon_i| < \epsilon$. We want to verify that

$$\phi(\bar{Y}, X) > \phi(Y, X) \approx -0.48. \quad (17)$$

There are two possibilities. **Possibility 1:** $\epsilon_1 = 0$ or $\epsilon_2 = 0$. WLOG, assume $\epsilon_1 = 0$, then we must have $\epsilon_2 > 0$. Then we still have $y_1 = \bar{y}_1 = x_1$. Since the perturbation amount is small enough, we have $y_2 \notin \{x_1, x_2\}$. According to Case 2 above, we have $\phi(\bar{Y}, X) = -\log 2 \approx -0.35 > -0.48$.

Possibility 2: $\epsilon_1 > 0, \epsilon_2 > 0$. Since the perturbation amount ϵ_1 and ϵ_2 are small enough, we have $y_1 \notin \{x_1, x_2\}, y_2 \notin \{x_1, x_2\}$. According to Case 4 above, we have $\phi(\bar{Y}, X) = 0 > -0.48$. Combining both cases, we have proved Eq. (17). \square

H.2 Proof of Claim 3.2 (for RS-GAN)

This is the result of RS-GAN for $n = 2$. WLOG, assume $x_1 = 0, x_2 = 1$. Denote $g_{\text{RS}}(Y) \triangleq \phi_{\text{RS}}(Y, X) = \sup_{f \in C(\mathbb{R}^d)} \frac{1}{2} \log \frac{1}{1 + \exp(f(0) - f(y_1))} + \frac{1}{2} \log \frac{1}{1 + \exp(f(1) - f(y_2))}$. Denote $m_i = |\{y_i\} \cap \{x_i\}|, i = 1, 2$; note this definition is different from JS-GAN in App. H.1. Consider three cases.

Case 1: $m_1 = m_2 = 1$. If $y_1 = 0, y_2 = 1$, then $g_{\text{RS}}(Y) = \frac{1}{2}[\log 0.5 + \log 0.5] = -\log 2 \approx -0.6937$. If $y_1 = 1, y_2 = 0$, then

$$\begin{aligned} g_{\text{RS}}(Y) &= \sup_{f \in \mathcal{F}} \frac{1}{2} \log \frac{1}{1 + \exp(f(0) - f(1))} + \frac{1}{2} \log \frac{1}{1 + \exp(f(1) - f(0))} \\ &= \sup_{t \in \mathbb{R}} \left[\frac{1}{2} \log \frac{1}{1 + \exp(t)} + \frac{1}{2} \log \frac{1}{1 + \exp(-t)} \right] = -\log 2. \end{aligned}$$

Case 2: $\{m_1, m_2\} = \{0, 1\}$. WLOG, assume $y_1 = 0, y_2 \neq 1$ (note that y_2 can be 0). Then

$$\begin{aligned} g_{\text{RS}}(Y) &\geq \sup_{f \in \mathcal{F}} \frac{1}{2} \log \frac{1}{1 + \exp(f(0) - f(0))} + \frac{1}{2} \log \frac{1}{1 + \exp(f(1) - f(y_2))} \\ &= -\frac{1}{2} \log 2 + \sup_{t \in \mathbb{R}} \frac{1}{2} \log \frac{1}{1 + \exp(t)} = -\frac{1}{2} \log 2 \approx -0.3466. \end{aligned}$$

The value is achieved when $f(1) - f(y_2) \rightarrow -\infty$.

Case 3: $m_1 = m_2 = 0$. Then

$$\begin{aligned} g_{\text{RS}}(Y) &\geq \sup_{f \in \mathcal{F}} \frac{1}{2} \log \frac{1}{1 + \exp(f(0) - f(y_1))} + \frac{1}{2} \log \frac{1}{1 + \exp(f(1) - f(y_2))} \\ &= \sup_{t_1 \in \mathbb{R}, t_2 \in \mathbb{R}} \frac{1}{2} \log \frac{1}{1 + \exp(t_1)} + \frac{1}{2} \log \frac{1}{1 + \exp(t_2)} = 0. \end{aligned}$$

The value is achieved when $f(1) - f(y_2) \rightarrow -\infty$ and $f(0) - f(y_1) \rightarrow -\infty$.

The global minimal value is $-\log 2$, and the only global minima are $\{y_1, y_2\} = \{x_1, x_2\}$. In addition, from any Y , it is easy to verify that there is a non-decreasing path from Y to a global minimum.

H.3 Proofs for 2-Cluster Data (Possibly Imbalanced)

Proof of Claim C.1. The proof is built on the proof of Claim 3.1 in Appendix H.1.

We first consider a special case $|\mathcal{X}_1 \cap \mathcal{Y}|=m, |\mathcal{X}_2 \cap \mathcal{Y}|=0$. This means that m generated points are in mode 1, and the rest are in neither modes. The loss value can be computed as follows:

$$\begin{aligned}\phi_{\text{JS}}(Y, X) &= \frac{1}{2n} \left[\alpha n \log\left(\frac{\alpha n}{\alpha n + m}\right) + m \log\left(1 - \frac{\alpha n}{\alpha n + m}\right) \right] \\ &= \frac{\alpha}{2} \log(\alpha n) + \frac{m}{2n} \log m - \frac{\alpha n + m}{2n} \log(\alpha n + m) = q_\alpha(m).\end{aligned}$$

In general, if $|\mathcal{X}_1 \cap \mathcal{Y}|=m_1, |\mathcal{X}_2 \cap \mathcal{Y}|=m_2$, then $\phi_{\text{JS}}(Y, X)$ can be divided into three parts: the first part is the sum of the terms that contain x_1 (including x_i 's and y_j 's that are equal to x_1), the second part is the sum of the terms that contain x_n (including x_i 's and y_j 's that are equal to x_n), and the third part is the sum of the terms that contain y_j 's that are not in $\{x_1, x_n\}$. Similar to Case 3 above, the value of the first part is $q_\alpha(m_1)$, and the value of the second part is $q_{1-\alpha}(m_2)$. Similar to the above special case, the value of the third part is 0. Therefore, the loss value is $\phi_{\text{JS}}(Y, X) = q_\alpha(m_1) + q_{1-\alpha}(m_2)$.

It is easy to show that $q_\alpha(m_1) + q_{1-\alpha}(m_2) \geq -\log 2$, and the equality is achieved iff $m_1 = n\alpha, m_2 = n(1 - \alpha)$, i.e., $\mathcal{Y} = \mathcal{X}_1 \cup \mathcal{X}_2$. \square

Proof sketch of Corollary C.1. After a small enough perturbation, we must have $m_1 \triangleq |\mathcal{X}_2 \cap \mathcal{Y}| \leq n_1, m_2 \triangleq |\mathcal{X}_1 \cap \mathcal{Y}| \leq n_2$. Since $q_\alpha(m)$ and $q_{1-\alpha}(m)$ are strictly decreasing functions of m , we have

$$\phi(Y, X) = q_\alpha(m_1) + q_{1-\alpha}(m_2) \leq q_\alpha(n_1) + q_{1-\alpha}(n_2) = \phi(\hat{Y}, X).$$

The equality holds iff $(m_1, m_2) = (n_1, n_2)$, i.e., $Y = \hat{Y}$. This means that if $(n_1, n_2) \neq (n\alpha, n(1 - \alpha))$, then \hat{Y} is a sub-optimal strict local minimum. \square

We skip the detailed proof, since other parts are similar to the proof of Corollary 3.1.

I Proof of Theorem 1 (Landscape of Separable-GAN)

Denote $F(D; Y) = \frac{1}{2n} \sum_{i=1}^n [h_1(f(x_i)) + h_2(-f(y_i))] \leq 0$ (since $h_i(t) \leq 0, i = 1, 2$ for any t).

Step 1: Compute the value of $\phi(\cdot, X)$ for each Y . For any i , denote $M_i = \{j : y_j = x_i\}, m_i = |M_i| \geq 0, i = 1, 2, \dots, n$. Then $m_1 + \dots + m_n = n$. Denote $\Omega = M_1 \cup M_2 \dots \cup M_n$. Then

$$\begin{aligned}\phi(Y, X) &= \frac{1}{2n} \sup_f \sum_{i=1}^n [h_1(f(x_i)) + h_2(-f(y_i))] = \frac{1}{2n} \sup_f \left(\sum_{i=1}^n [h_1(f_1(x_i)) + m_i h_2(-f(x_i))] + \sum_{j \notin \Omega} h_2(-f(y_j)) \right) \\ &\stackrel{(i)}{=} \frac{1}{2n} \left(\sum_{i=1}^n \sup_{t_i \in \mathbb{R}} [h_1(t_i) + m_i h_2(-t_i)] + |\Omega^c| \sup_{t \in \mathbb{R}} h_2(t) \right) \stackrel{(ii)}{=} \frac{1}{2n} \sum_{i=1}^n \xi(m_i) \\ &\stackrel{(iii)}{\geq} \frac{1}{2n} \sum_{i=1}^n m_i \xi(1) = \frac{1}{2} \xi(1).\end{aligned}\tag{18a}$$

Here (i) is because $f(y_j), j \in \Omega$ are independent of $h(x_i)$'s and thus can be any values; (ii) is by the definition $\xi(m) = \sup_t [h_1(t) + m h_2(-t)]$ and Assumption 4.1 that $\sup_t h_2(t) = 0$; (iii) is due to the convexity of ξ (note that ξ is the supreme of linear functions). Furthermore, if there is a certain $m_i > 1$, then $\xi(m_i) + (m_i - 1)\xi(0) = \xi(m_i) > m_i \xi(1)$ (according to Assumption 4.2), causing (iii) to become a strict inequality. Thus the equality in (iii) holds iff $m_i = 1, \forall i$, i.e., $\{y_1, \dots, y_n\} = \{x_1, \dots, x_n\}$. Therefore, we have proved that $\phi(Y, X)$ achieves the minimal value $\frac{1}{2} \xi(1)$ iff $\{y_1, \dots, y_n\} = \{x_1, \dots, x_n\}$.

Step 2: Sufficient condition for strict local-min. Next, we show that if Y satisfies $m_1 + m_2 + \dots + m_n = n$ then Y is a strict local-min. Denote $\delta = \min_{k \neq l} \|x_k - x_l\|$. Consider a small perturbation of Y as $\bar{Y} = (\bar{y}_1, \bar{y}_2, \dots, \bar{y}_n) = (y_1 + \epsilon_1, y_2 + \epsilon_2, \dots, y_n + \epsilon_n)$, where $\|\epsilon_j\| < \delta, \forall j$ and $\sum_j \|\epsilon_j\|^2 > 0$. We want to prove $\phi(\bar{Y}, X) > \phi(Y, X)$.

Denote $\bar{m}_i = |\{j : \bar{y}_j = x_i\}|, i = 1, 2, \dots, n$. Consider an arbitrary j . Since $y_j \in \{x_1, \dots, x_n\}$, there must be some i such that $y_j = x_i$. Together with $\|\bar{y}_j - y_j\| = \|\epsilon_j\| < \delta = \min_{k \neq l} \|x_k - x_l\|$, we have $\bar{y}_j \notin (\{x_1, x_2, \dots, x_n\} \setminus \{x_i\})$. In other words, the only possible point in $\{x_1, \dots, x_n\}$ that can coincide with \bar{y}_j is x_i , and this happens only when $\epsilon_j = 0$. This implies $\bar{m}_i \leq m_i, \forall i$. Since

we have assumed $\sum_j \|\epsilon_j\|^2 > 0$, for at least one i we have $\bar{m}_i < m_i$. Together with Assumption 4.3 that $\xi(m)$ is a strictly decreasing function in $m \in [0, n]$, we have $\phi(\bar{Y}, X) = \frac{1}{n} \sum_{i=1}^n \xi(\bar{m}_i) > \frac{1}{n} \sum_{i=1}^n \xi(m_i) = \phi(Y, X)$.

Step 3: Sub-optimal strict local-min. Finally, if Y satisfies that $m_1 + m_2 + \dots + m_n = n$ and $m_k \geq 2$ for some k , then $\phi(Y, X) > \frac{1}{2}\xi(0)$. Thus Y is a sub-optimal strict local minimum. **Q.E.D.**

Remark 1: $\xi(m)$ is convex (it is the supreme of linear functions), thus we always have $\xi(m) = \xi(m) + (m-1)\xi(0) \geq m\xi(1)$. Assump. 4.2 states that the inequality is strict, thus it is slightly stronger than the convexity of ξ . By Assump. 4.1, we also have $h_1(t) + (m+1)h_2(-t) \leq h_1(t) + mh_2(-t)$, thus $\xi(n) \leq \xi(n-1) \leq \dots \leq \xi(0)$. Assumption 4.3 states that the inequalities are strict. This holds if the maximizer of $h_1(t) + mh_2(-t)$ does not coincide with the maximizer of $h_2(t)$. Intuitively, if $h(t)$ is ‘‘substantially different’’ from a constant function, then Assump. 4.2 and Assump. 4.3 hold.

Remark 2: The upper bound 0 in Assumption 4.1 is not essential, and can be relaxed to any finite numbers (change other two assumptions accordingly). We skip the details.

J Proof of Theorem 2 (Landscape of RpGAN)

This proof is the longest one in this paper. We will focus on a proof for the special case of RS-GAN. The proof for general RpGAN is quite similar, and presented in Appendix J.3. Recall $\phi_{\text{RS}}(Y, X) = \sup_f \frac{1}{n} \sum_{i=1}^n \log \frac{1}{1 + \exp(f(y_i) - f(x_i))}$.

Theorem J.1. (special case of Theorem 2 for RS-GAN) Suppose $x_1, x_2, \dots, x_n \in \mathbb{R}^d$ are distinct. The global minimal value of $\phi_{\text{RS}}(Y, X)$ is $-\log 2$, which is achieved iff $\{x_1, \dots, x_n\} = \{y_1, \dots, y_n\}$. Furthermore, any point is global-min-reachable for the function.

Proof sketch. We compute the value of $g(Y) = \phi_{\text{RS}}(Y, X)$ for any Y , using the following steps:

- (i) We build a graph with vertices representing distinct values of x_i, y_i and draw directed edges from x_i to y_i . This graph can be decomposed into cycles and trees.
- (ii) Each vertex in a cycle contributes $-\frac{1}{n} \log 2$ to the value $g(Y)$.
- (iii) Each vertex in a tree contributes 0 to the value $g(Y)$.
- (iv) The value $g(Y)$ equals $-\frac{1}{n} \log 2$ times the number of vertices in the cycles.

The outline of this section is as follows. In the first subsection, we analyze an example as warm-up. Next, we prove Theorem J.1. The proofs of some technical lemmas will be provided in the following subsections. Finally, in Appendix J.3 we present the proof for Theorem 2.

J.1 Warm-up Example

We prove that if $\{y_1, y_2, \dots, y_n\} = \{x_1, \dots, x_n\}$, then Y is a global minimum of $g(Y)$.

Suppose $y_i = x_{\sigma(i)}$, where $(\sigma(1), \sigma(2), \dots, \sigma(n))$ is a permutation of $(1, 2, \dots, n)$. We can divide $\{1, 2, \dots, n\}$ into finitely many cycles C_1, C_2, \dots, C_K , where each cycle $C_k = (c_k(1), c_k(2), \dots, c_k(m_k))$ satisfies $c_k(j+1) = \sigma(c_k(j))$, $j \in \{1, 2, \dots, m_k\}$. Here $c_k(m_k+1)$ is defined as $c_k(1)$. Now we calculate the value of $g(Y)$.

$$\begin{aligned}
g(Y) &= \sup_f \frac{1}{n} \sum_{i=1}^n \log \frac{1}{1 + \exp(f(y_i) - f(x_i))} \stackrel{(i)}{=} - \inf_f \frac{1}{n} \sum_{k=1}^K \sum_{i \in C_k} \log(1 + \exp(f(y_i) - f(x_i))) \\
&= - \inf_f \frac{1}{n} \sum_{k=1}^K \sum_{j=1}^{m_k} \log(1 + e^{f(x_{c_k(j+1)}) - f(x_{c_k(j)})}) \stackrel{(ii)}{=} - \frac{1}{n} \sum_{k=1}^K \inf_f \sum_{j=1}^{m_k} \log(1 + e^{f(x_{c_k(j+1)}) - f(x_{c_k(j)})}) \\
&= - \frac{1}{n} \sum_{k=1}^K \inf_{t_1, t_2, \dots, t_{m_k} \in \mathbb{R}} \left[\sum_{j=1}^{m_k-1} \log(1 + \exp(t_{j+1} - t_j)) + \log(1 + \exp(t_1 - t_{m_k})) \right] \\
&\stackrel{(iii)}{=} - \frac{1}{n} \sum_{k=1}^K m_k \log(1 + \exp(0)) = - \log 2.
\end{aligned}$$

Here (i) is because $\{1, 2, \dots, n\}$ is the combination of C_1, \dots, C_K and $i \in C_k$ means that $i = c_k(j)$ for some j . (ii) is because C_k 's are disjoint and f can be any continuous function; more specifically,

the choice of $\{f(x_i) : i \in C_k\}$ is independent of the choice of $\{f(x_i) : i \in C_l\}$ for any $k \neq l$, thus we can take the infimum over each cycle (i.e., put “inf” inside the sum over k). (iii) is because $\sum_{j=1}^{m-1} \log(1 + \exp(t_{j+1} - t_j)) + \log(1 + \exp(t_1 - t_m))$ is a convex function of t_1, t_2, \dots, t_m and the minimum is achieved at $t_1 = t_2 = \dots = t_m = 0$.

J.2 Proof of Theorem J.1

This proof is divided into three steps. In Step 1, we compute the value of $g(Y)$ if all $y_i \in \{x_1, \dots, x_n\}$. This is the major step of the whole proof. In Step 2, we compute the value of $g(Y)$ for any Y . In Step 3, we show that there is a non-decreasing continuous path from Y to a global minimum.

Step 1: Compute $g(Y)$ that all $y_i \in \{x_1, \dots, x_n\}$. Define

$$R(X) = \{Y : y_i \in \{x_1, \dots, x_n\}, \forall i\}. \quad (19)$$

Step 1.1: Build a graph and decompose it. We fix $Y \in R(X)$. We build a directed graph $G = (V, A)$ as follows. The set of vertices $V = \{1, 2, \dots, n\}$ represent x_1, x_2, \dots, x_n . A directed edge $(i, j) \in A$ if $y_i = x_j$. In this case, there is a term $\log(1 + \exp(f(x_j) - f(x_i)))$ in $g(Y)$. It is possible to have a self-loop (i, i) , which corresponds to the case $y_i = x_i$. By Eq. (19), we have

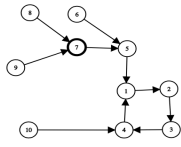
$$g(Y) = -\inf_f \frac{1}{n} \sum_{i=1}^n \log(1 + e^{f(y_i) - f(x_i)}) = -\inf_f \frac{1}{n} \sum_{(i,j) \in A} \log(1 + e^{f(x_j) - f(x_i)}). \quad (20)$$

Each y_i corresponds to a unique x_j , thus the out-degree of i , denoted as $\text{outdegree}(i)$, must be exactly 1. The in-degree of each i , denoted as $\text{indegree}(i)$, can be any number in $\{0, 1, \dots, n\}$.

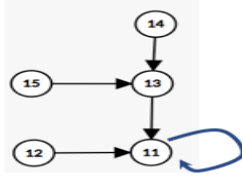
We will show that the graph G can be decomposed into the union of cycles and trees (see App. J.2.1 for its proof, and definitions of cycles and trees). A graphical illustration is given in Figure 25.

Lemma 1. *Suppose $G = (V, A)$ is a directed graph and $\text{outdegree}(v) = 1, \forall v \in V$. Then:*

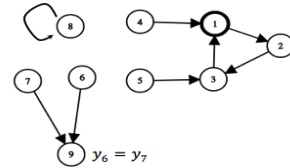
- (a) *There exist cycles C_1, C_2, \dots, C_K and subtrees T_1, T_2, \dots, T_M such that each edge $v \in A$ appears either in exactly one of the cycles or in exactly one of the subtrees.*
- (b) *The root of each subtree u_m is a vertex of a certain cycle C_k . In addition, each vertex of the graph appears in exactly one of the following sets: $V(C_1), \dots, V(C_K), V(T_1) \setminus \{u_1\}, \dots, V(T_M) \setminus \{u_M\}$.*
- (c) *There is at least one cycle in the graph.*



(a) Eg 1 for Lemma 1



(b) Eg 2, with self-loop



(c) Example graph for general case

Figure 25: The first two figures are two connected component of a graph representing the case $y_i \in \{x_1, \dots, x_n\}, \forall i$. The first figure contains 10 vertices and 10 directed edges. It can be decomposed into a cycle $(1, 2, 3, 4)$ and two subtrees: one subtree consists of edge $(10, 4)$ and vertices 10, 4, and another consists of edges $(8, 7), (9, 7), (7, 5), (6, 5), (5, 1)$. The second figure has one cycle being a self-loop, and two trees attached to it. The third figure is an example graph of the case that some $y_i \notin \{x_1, \dots, x_n\}$. In this example, $n = 8$ (so 8 edges), and all y_i 's are in $\{x_1, \dots, x_n\}$ except y_6, y_7 . The two edges $(6, 9)$ and $(7, 9)$ indicate the two terms $h(f(y_6) - f(x_6))$ and $h(f(y_7) - f(x_7))$ in $g(Y)$. They have the same head 9, thus $y_6 = y_7$. The vertex 9 has out-degree 0, indicating that $y_6 = y_7 \notin \{x_1, \dots, x_n\}$. This figure can be decomposed into two cycles and three subtrees. Finally, adding a self-loop $(9, 9)$ will generate a graph where each edge has outdegree 1 (this is the reduction done in Step 2).

Denote $\xi(y_i, x_i) = \log(1 + e^{f(y_i) - f(x_i)})$. According to Lemma 1, we have

$$-ng(Y) = \inf_f \sum_{i=1}^n \xi(y_i, x_i) \geq \inf_f \left[\sum_{k=1}^K \sum_{i \in V(C_k)} \xi(y_i, x_i) \right] \triangleq g_{\text{cyc}}. \quad (21)$$

Step 1.2: Compute g_{cyc} . We then compute g_{cyc} . Since C_k is a cycle, we have $X_k \triangleq \{x_i : i \in C_k\} = \{y_i : i \in C_k\}$. Since C_k 's are disjoint, we have $X_k \cap X_l = \emptyset, \forall k \neq l$. This implies that

$f(x_i), f(y_i)$ for i in one cycle C_k are independent of the values corresponding to other cycles. Then g_{cyc} can be decomposed according to different cycles:

$$g_{\text{cyc}} = \inf_f \left[\sum_{k=1}^K \sum_{i \in V(C_k)} \log(1 + \exp(f(y_i) - f(x_i))) \right] = \sum_{k=1}^K \inf_f \sum_{i \in V(C_k)} \log(1 + \exp(f(y_i) - f(x_i))).$$

Similar to Warm-up example 1, the infimum for each cycle is achieved when $f(x_i) = f(x_j), \forall i, j \in V(C_k)$. In addition,

$$g_{\text{cyc}} = -\log 2 \sum_{k=1}^K |V(C_k)|. \quad (22)$$

Step 1.3: Compute $g(Y)$. According to Eq. (21) and Eq. (22), we have

$$-ng(Y) \geq \sum_{k=1}^K |V(C_k)| \log 2. \quad (23)$$

Denote $F(Y; f) = -\frac{1}{n} \sum_{i=1}^n \log(1 + e^{f(y_i) - f(x_i)})$, then $g(Y) = \inf_f F(Y; f)$. We claim that for any $\epsilon > 0$, there exists a continuous function f such that

$$-nF(Y; f) < \sum_{k=1}^K |V(C_k)| \log 2 + \epsilon. \quad (24)$$

Let N be a large positive number such that

$$n \log(1 + \exp(-N)) < \epsilon. \quad (25)$$

Pick a continuous function f as follows.

$$f(x_i) = \begin{cases} 0, & i \in \bigcup_{k=1}^K V(C_k), \\ N \cdot \text{depth}(i), & i \in \bigcup_{m=1}^M V(T_m). \end{cases} \quad (26)$$

Note that the root u_m of a tree T_m is also in a certain cycle C_k , thus the value $f(x_{u_m})$ is defined twice in Eq. (26), but in both definitions its value is 0, thus the definition of f is valid. For any $i \in V(C_k)$, suppose $y_i = x_j$, then both $i, j \in V(C_k)$ which implies $f(y_i) - f(x_i) = f(x_j) - f(x_i) = 0$. For any $i \in V(T_m) \setminus \{u_m\}$, suppose $y_i = x_j$, then by the definition of the graph (i, j) is a directed edge of the tree T_m , which means that $\text{depth}(i) = \text{depth}(j) + 1$. Thus $f(y_i) - f(x_i) = f(x_j) - f(x_i) = -N$. In summary, for the choice of f in Eq. (26), we have

$$f(y_i) - f(x_i) = \begin{cases} 0, & i \in \bigcup_{k=1}^K V(C_k), \\ -N, & i \in \bigcup_{m=1}^M V(T_m). \end{cases} \quad (27)$$

Denote $p = \sum_{k=1}^K |V(C_k)| \log 2$. For the choice of f in Eq. (26), we have

$$\begin{aligned} -nF(Y; f) &= \sum_{i=1}^n \log(1 + e^{f(y_i) - f(x_i)}) \\ &= \left[\sum_{k=1}^K \sum_{i \in V(C_k)} \log(1 + e^{f(y_i) - f(x_i)}) + \sum_{m=1}^M \sum_{i \in V(T_m) \setminus \{u_m\}} \log(1 + e^{f(y_i) - f(x_i)}) \right] \\ &\stackrel{(27)}{=} \left[\sum_{k=1}^K \sum_{i \in V(C_k)} \log(1 + e^0) + \sum_{m=1}^M \sum_{i \in V(T_m) \setminus \{u_m\}} \log(1 + e^{-N}) \right] \\ &= \sum_{k=1}^K |V(C_k)| \log 2 + \sum_{k=1}^M (|V(T_m)| - 1) \log(1 + e^{-N}) \leq p + n \log(1 + e^{-N}) \stackrel{(25)}{<} p + \epsilon. \end{aligned} \quad (28)$$

This proves Eq. (24). Combining the two relations given in Eq. (24) and Eq. (23), we have

$$g(Y) = \inf_f F(Y; f) = \frac{1}{n} \sum_{k=1}^K |V(C_k)| \log 2, \quad \forall Y \in R(X). \quad (29)$$

Step 2: Compute $g(Y)$ for any Y .

In the general case, not all y_i 's lie in $\{x_1, \dots, x_n\}$. We will reduce to the previous case. Denote

$$H = \{i : y_i \in \{x_1, \dots, x_n\}\}, \quad H^c = \{j : y_j \notin \{x_1, \dots, x_n\}\}.$$

Since y_j 's in H^c may be the same, we define the set of such distinct values of y_j 's as

$$Y_{\text{out}} = \{y \in \mathbb{R}^d : y = y_j, \text{ for some } j \in H^c\}.$$

Let $\bar{n} = |Y_{\text{out}}|$, then there are total $n + \bar{n}$ distinct values in $x_1, \dots, x_n, y_1, \dots, y_n$. WLOG, assume $y_1, \dots, y_{\bar{n}}$ are distinct (this is because the value of $g(Y)$ does not change if we re-index x_i 's and y_i 's as long as the subscripts of x_i, y_i change together), then

$$Y_{\text{out}} = \{y_1, \dots, y_{\bar{n}}\}.$$

We create artificial ‘‘true data’’ and ‘‘fake data’’ $x_{n+1} = x_{n+1} = y_1, \dots, x_{n+\bar{n}} = y_{n+\bar{n}} = y_{\bar{n}}$. Define $F_{\text{auc}}(Y, f) = -\sum_{i=1}^{n+\bar{n}} \log(1 + e^{f(y_i) - f(x_i)})$, $g_{\text{auc}} = -\inf_f F_{\text{auc}}(Y, f)$. Clearly, $F_{\text{auc}}(Y, f) = nF(Y, f) - \bar{n} \log 2$ and $ng(Y) = g_{\text{auc}} - \bar{n} \log 2$.

Consider the new configurations $\hat{X} = (x_1, \dots, x_{n+\bar{n}})$ and $\hat{Y} = (y_1, \dots, y_{n+\bar{n}})$. For the new configurations, we can build a graph \hat{G} with $n + \bar{n}$ vertices and $n + \bar{n}$ edges. There are K self-loops $C_{K+1}, \dots, C_{K+\bar{n}}$ at the vertices corresponding to $y_1, \dots, y_{\bar{n}}$. Based on Lemma 1, we have: (a) There exist cycles $C_1, C_2, \dots, C_K, C_{K+1}, \dots, C_{K+\bar{n}}$ and subtrees T_1, T_2, \dots, T_M (with roots u_m 's) s.t. each edge $v \in A$ appears in exactly one of the cycle or subtrees. (b) u_m is a vertex of a certain cycle C_k where $1 \leq k \leq K + \bar{n}$. (c) Each vertex of the graph appears in exactly one of the following sets: $V(C_1), \dots, V(C_{K+\bar{n}}), V(T_1) \setminus \{u_1\}, \dots, V(T_M) \setminus \{u_M\}$. According to the proof in Step 1, we have $g_{\text{auc}} = \sum_{k=1}^{K+\bar{n}} |V(C_k)| \log 2 = \sum_{k=1}^K |V(C_k)| \log 2 + \bar{n} \log 2$. Therefore,

$$ng(Y) = g_{\text{auc}} - \bar{n} \log 2 = \sum_{k=1}^K |V(C_k)| \log 2.$$

We build a graph G by removing the self-loops $C_{K+j} = (y_j, y_j), j = 1, \dots, \bar{n}$ in \hat{G} . The new graph G consists of $n + \bar{n}$ vertices corresponding to x_1, \dots, x_n and $y_1, \dots, y_{\bar{n}}$ and n edges. The graph can be decomposed into cycles C_1, C_2, \dots, C_K (since \bar{n} cycles are removed from \hat{G}) and subtrees T_1, T_2, \dots, T_M . The value $ng(Y) = \sum_{k=1}^K |V(C_k)| \log 2$, where C_k 's are all the cycles of G .

Step 3: Finding a non-decreasing path to a global minimum. Finally, we prove that for any Y , there is a non-decreasing continuous path from Y to one global minimal Y^* . The following claim shows that we can increase the value of Y incrementally. See the proof in Appendix J.2.2.

Claim J.1. *For an arbitrary Y that is not a global minimum, there exists another \hat{Y} and a non-decreasing continuous path from Y to \hat{Y} such that $g(\hat{Y}) - g(Y) \geq \frac{1}{n} \log 2$.*

For any Y that is not a global minimum, we apply Claim J.1 for finitely many times (no more than n times), then we will arrive at one global minimum Y^* . We connect all non-decreasing continuous paths and get a non-decreasing continuous path from Y to Y^* . This finishes the proof.

J.2.1 Graph Preliminaries and Proof of Lemma 1

We present a few definitions from standard graph theory.

Definition J.1. (walk, path, cycle) *In a directed graph $G = (V, A)$, a walk $W = (v_0, e_1, v_1, e_2, \dots, v_{m-1}, e_m, v_m)$ is a sequence of vertices and edges such that $v_i \in V, \forall i \in \{0, 1, \dots, m\}$ and $e_i = (v_{i-1}, v_i) \in A, \forall i \in \{1, \dots, m\}$. If v_0, v_1, \dots, v_m are distinct, we call it path (with length m). If v_0, v_1, \dots, v_{m-1} are distinct and $v_m = v_0$, we call it a cycle.*

Any v has a path to itself (with length 0), no matter whether there is an edge between v to itself or not. This is because the degenerate walk $W = (v)$ satisfies the above definition. The set of vertices and edges in W are denoted as $V(W)$ and $A(W)$ respectively.

Definition J.2. (tree) A directed tree is a directed graph $T = (V, A)$ with a designated node $r \in V$, the root, such that there is exactly one path from v to r for each node $v \in V$ and there is no edge from the root r to itself. The depth of a node is the length of the path from the node to the root (the depth of the root is 0). A subtree of a directed graph G is a subgraph T which is a directed tree.

Proof of Lemma 1:

We slightly extend the definition of “walk” to allow infinite length. We present two observations.

Observation 1: Starting from any vertex $v_0 \in V(G)$, there is a unique walk with infinite length

$$W(v_0) \triangleq (v_0, e_1, v_1, e_2, v_2, \dots, v_i, e_i, v_{i+1}, e_{i+1}, \dots),$$

where e_i is an edge in $A(G)$ with tail v_{i-1} and head v_i .

Proof of Observation 1: At each vertex v_i , there is a unique outgoing edge $e_i = (v_i, v_{i+1})$ which uniquely defines the next vertex v_{i+1} . Continue the process, we have proved Observation 1.

Observation 2: The walk $W(v_0) \triangleq (v_0, e_1, v_1, e_2, v_2, \dots, v_i, e_i, v_{i+1}, e_{i+1}, \dots)$ can be decomposed into two parts $W_1(v_0) = (v_0, e_1, v_1, e_2, v_2, \dots, v_{i_0-1}, e_{i_0-1}, v_{i_0})$, $W_2(v_0) = (v_{i_0}, e_{i_0+1}, v_{i_0+1}, e_{i_0+2}, v_{i_0+2}, \dots)$, where $W_1(v_0)$ is a path from v_0 to v_{i_0} (i.e. v_0, v_1, \dots, v_{i_0} are distinct), and $W_2(v_0)$ is the repetition of a certain cycle (i.e., there exists T such that $v_{i+T} = v_i$, for any $i \geq i_0$). This decomposition is unique, and we say the “first-touch-vertex” of v_0 is v_{i_0} .

Proof of Observation 2: Since the graph is finite, then some vertices must appear at least twice in $W(v_0)$. Among all such vertices, suppose u is the one that appears the earliest in the walk $W(v_0)$, and the first two appearances are $v_{i_0} = u$ and $v_{i_1} = u$ and $i_0 < i_1$. Denote $T = i_1 - i_0$. Then it is easy to show $W_2(v_0)$ is the repetitions of the cycle consisting of vertices $v_{i_0}, v_{i_0+1}, \dots, v_{i_1-1}$, and $W_1(v_0)$ is a directed path from v_0 to v_{i_0} .

The first-touch-vertex $u = v_{i_0}$ has the following properties: (i) $u \in C_k$ for some k ; (ii) there exists a path from v to u ; (iii) any paths from v to any vertex in the cycle C_k other than u must pass u . Note that if u is in some cycle, then its first-touch-vertex is u itself.

As a corollary of Observation 2, there is at least one cycle. Suppose all cycles of G are C_1, C_2, \dots, C_K . Because the outdegree of each vertex is 1, these cycles must be disjoint, i.e., $V(C_i) \cap V(C_j) = \emptyset$ and $A(C_i) \cap A(C_j) = \emptyset$, for any $i \neq j$. Denote the set of vertices in the cycles as

$$V_c = \bigcup_{k=1}^K V(C_1) \cup \dots \cup V(C_K). \quad (30)$$

Let u_1, \dots, u_M be the vertices of C_1, \dots, C_m with indegree at least 2.

Based on Observation 2, starting from any vertex outside V_c there is a unique path that reaches V_c . Combining all vertices that reach the cycles at u_m (denoted as V_m), and the paths from these vertices to u_m , we obtain a directed subgraph T_m , which is connected with V_c only via the vertex u_m . The subgraphs T_m 's are disjoint from each other since they are connected with V_c via different vertices. In addition, each vertex outside of V_c lies in exactly one of the subgraph T_m . Thus, we can partition the whole graph into the union of the cycles C_1, \dots, C_K and the subgraphs T_1, \dots, T_M .

We then show T_m 's are trees. For any vertex v_0 in the subgraph T_m , consider the walk $W(v_0)$. Any path starting from v_0 must be part of $W(v_0)$. Starting from v_0 there is only one path from v_0 to u_m which is $W_1(v_0)$, according to Observation 2. Therefore, by the definition of a directed tree, T_m is a directed tree with the root u_m . Therefore, we can partition the whole graph into the union of the cycles C_1, \dots, C_K and subtrees T_1, \dots, T_M with disjoint edge sets; in addition, the edge sets of the cycles are disjoint, and the root of T_l must be in certain cycle C_k . It is easy to verify the properties stated in Lemma 1. This finishes the proof.

J.2.2 Proof of Claim J.1

We first prove the case for $d \geq 2$. Suppose the corresponding graph for Y is G , and G is decomposed into the union of cycles C_1, \dots, C_K and trees T_1, \dots, T_m . We perform the following operation: pick an arbitrary tree T_m with the root u_m . The tree is non-empty, thus there must be an edge e with the head u_m .

Suppose v is the tail of the edge e . Now we remove the edge $e = (v, u_m)$ and create a new edge $e' = (v, v)$. The new edge corresponds to $y_v = x_v$. The old edge (v, u_m) corresponds to

$y_v = x_{u_m}$ (and a term $h(f(x_{u_m}) - f(x_v))$) if $u_m \leq n$ or $y_v = y_{u_m-n} \notin \{x_1, \dots, x_n\}$ (and a term $h(f(y_{u_m-n}) - f(x_v))$) if $u_m > n$. This change corresponds to the change of y_v : we change $y_v = x_{u_m}$ (if $u_m \leq n$) or $y_v = y_{u_m-n}$ (if $u_m > n$) to $\hat{y}_v = x_v$. Let $\hat{y}_i = y_i$ for any $i \neq v$, and $\hat{Y} = (\hat{y}_1, \dots, \hat{y}_n)$ is the new point.

Previously v is in a tree T_m (not its root), now v is the root of a new tree, and also part of the new cycle (self-loop) $C_{K+1} = (v, e', v)$. In this new graph, the number of vertices in cycles increases by 1, thus the value of g increases by $-\frac{1}{n} \log 2$, i.e., $g(\hat{Y}) - g(Y) = \frac{1}{n} \log 2$.

Since $d \geq 2$, we can find a path in \mathbb{R}^d from a point to another point without passing any of the points in $\{x_1, \dots, x_n\}$. In the continuous process of moving y_v to \hat{y}_v , the function value will not change except at the end that $y_v = x_v$. Thus there is a non-increasing path from Y to \hat{Y} , in the sense that along this path the function value of g does not decrease.

The illustration of this proof is given below.

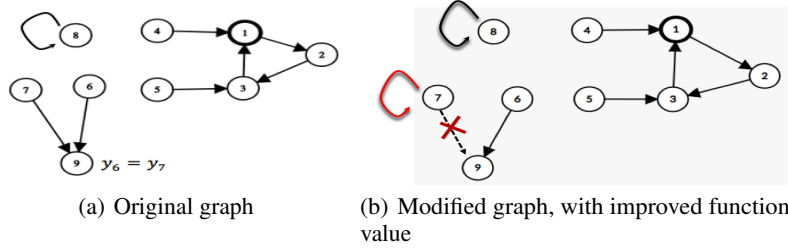


Figure 26: Illustration of the proof of Claim J.1. For the figure on the left, we pick an arbitrary tree with the head being vertex 9, which corresponds to $y_6 = y_7$. We change y_7 to $\hat{y}_7 = x_7$ to obtain the figure on the right. Since one more cycle is created, the function value increases by $-\frac{1}{n} \log 2$.

For the case $d = 1$, the above proof does not work. The reason is that the path from y_v to \hat{y}_v may touch other points in $\{x_1, \dots, x_n\}$ and thus may change the value of g . We only need to make a small modification: we move y_v in \mathbb{R} until it touches a certain x_i that corresponds to a vertex in the tree T_m , at which point a cycle is created, and the function value increases by at least $\frac{1}{n} \log 2$. This path is a non-decreasing path, thus the claim is also proved.

J.3 Proof of Theorem 2

Obviously, $g(Y) \triangleq \phi_{\mathbb{R}}(Y, X) = \frac{1}{n} \sup_{f \in C(\mathbb{R}^d)} \sum_{i=1}^n [h(f(x_i) - f(y_i))] \geq h(0)$ (by picking $f = 0$).

Step 1: achieving optimal $g(Y)$. We prove if $\{y_1, \dots, y_n\} = \{x_1, \dots, x_n\}$, then $g(Y) = h(0)$.

Claim J.2. Assume h is concave. Then the function $\xi_{\mathbb{R}}(m) = \sup_{(t_1, \dots, t_k) \in ZO(m)} \sum_{i=1}^m h(t_i)$ satisfies $\xi_{\mathbb{R}}(m) = mh(0)$, where the set $ZO(m) = \{t_1, t_2, \dots, t_m \in \mathbb{R} : \sum_{i=1}^m t_i = 0\}$.

The proof of this claim is obvious and skipped here. When $\{y_1, \dots, y_n\} = \{x_1, \dots, x_n\}$, we can divide $[n]$ into multiple cycles $C_1 \cup \dots \cup C_K$, each with length m_k , and obtain $\phi_{\mathbb{R}}(Y, X) = \frac{1}{n} \sup_{f \in C(\mathbb{R}^d)} \sum_{k=1}^K \sum_{i=1}^{m_k} [h(f(x_i) - f(y_i))] = \frac{1}{n} \sum_{k=1}^K \xi_{\mathbb{R}}(m_k) = \frac{1}{n} \sum_{k=1}^K m_k h(0) = h(0)$.

Step 2: compute $g(Y)$ when $y_i \in \{x_1, \dots, x_n\}, \forall i$. Assume $y_i \in \{x_1, \dots, x_n\}, \forall i$. We build a directed graph $G = (V, A)$ as follows (the same graph as in Appendix J.2). The set of vertices $V = \{1, 2, \dots, n\}$ represents x_1, x_2, \dots, x_n . We draw a directed edge $(i, j) \in A$ if $y_i = x_j$. Note that it is possible to have a self-loop (i, i) , which corresponds to the case $y_i = x_i$.

According to Lemma 1, this graph can be decomposed into cycles C_1, C_2, \dots, C_K and subtrees T_1, T_2, \dots, T_M . We claim that

$$\phi_{\mathbb{R}}(Y, X) = \frac{1}{n} \sum_{k=1}^K |V(C_k)| h(0) \geq h(0). \quad (31)$$

The proof of the relation in Eq. (31) is similar to the proof of Eq. (22) used in the proof of Theorem 2, and briefly explained below. One major part of the proof is to show that the contribution of the nodes

in the cycles is $\sum_{k=1}^K |V(C_k)|h(0)$. This is similar to Step 1, and is based on Claim J.2. Another major part of the proof is to show that the contribution of the nodes in the subtrees is zero, similar to the proof of Eq. (28). This is because we can utilize Assumption 4.4 to construct a sequence of f values (similar to Eq. (26)) so that

$$f(y_i) - f(x_i) = \begin{cases} 0, & i \in \bigcup_{k=1}^K V(C_k), \\ \alpha_N, & i \in \bigcup_{m=1}^M V(T_m). \end{cases} \quad (32)$$

Here $\{\alpha_N\}_{N=1}^\infty$ is a sequence of real numbers so that $\lim_{N \rightarrow \infty} h(\alpha_N) = \sup_t h(t) = 0$. In the case that $h(\infty) = 0$ like RS-GAN, we pick $\alpha_N = N$. In the case that $h(a) = 0$ for a certain finite number a , we can just pick $\alpha_N = a, \forall N$ (thus we do not need a sequence but just one choice).

Since the expression of $\phi_R(Y, X)$ in Eq. (31) is a scaled version of the expression of $\phi_{RS}(Y, X)$ (scale by $-\frac{\log 2}{h(0)}$), the rest of the proof is the same as the proof of Theorem 2.

Step 3: function value for general Y and GMR. This step is the same as the proof of Theorem J.1. For the value of general Y , we build an ‘‘augmented graph’’ and apply the result in Step 2 to obtain $g(Y)$. To prove GMR, the same construction as the proof of Theorem J.1 suffices.

K Results in Parameter Space

We will first state the technical assumptions and then present the formal results in parameter space. The results become somewhat technical due to the complication of neural-nets. Suppose the discriminator neural net is f_θ where $\theta \in \mathbb{R}^J$ and the generator net is G_w where $w \in \mathbb{R}^K$.

Assumption K.1. (*representation power of discriminator net*): For any distinct vectors $v_1, \dots, v_{2n} \in \mathbb{R}^d$, any $b_1, \dots, b_{2n} \in \mathbb{R}$, there exists $\theta \in \mathbb{R}^J$ such that $f_\theta(v_i) = b_i, i = 1, \dots, 2n$.

Assumption K.2. (*representation power of generator net in \mathcal{W}*): For any distinct $z_1, \dots, z_n \in \mathbb{R}^{d_z}$ and any $y_1, \dots, y_n \in \mathbb{R}^d$, there exists $w \in \mathcal{W}$ such that $G_w(z_i) = y_i, i = 1, \dots, n$.

For any given $Z = (z_1, \dots, z_n) \in \mathbb{R}^{d_z \times n}$, and any $Y \in \mathbb{R}^d \subseteq \mathbb{R}^K$, we define a set $G^{-1}(Y; Z)$ as follows: $w \in G^{-1}(Y; Z)$ iff $G_w(Z) = Y$ and $w \in \mathcal{W}$.

Assumption K.3. (*path-keeping property of generator net; duplication of Assumption 4.6*): For any distinct $z_1, \dots, z_n \in \mathbb{R}^{d_z}$, the following holds: for any continuous path $Y(t), t \in [0, 1]$ in the space $\mathbb{R}^{d \times n}$ and any $w_0 \in G^{-1}(Y(0); Z)$, there is continuous path $w(t), t \in [0, 1]$ such that $w(0) = w_0$ and $Y(t) = G_{w(t)}(Z), t \in [0, 1]$.

We will present sufficient conditions for these assumptions later. Next we present two main results on the landscape of GANs in the parameter space.

Proposition K.1. (*formal version of Proposition 1*): Consider the separable-GAN problem $\min_{w \in \mathbb{R}^K} \varphi_{\text{sep}}(w)$, where $\varphi_{\text{sep}}(w) = \sup_{\theta} \frac{1}{2n} \sum_{i=1}^n [h_1(f_\theta(x_i)) + h_2(-f_\theta(G_w(z_i)))]$. Suppose h_1, h_2 satisfy the same assumptions of Theorem 1. Suppose G_w satisfies Assumption K.2 and Assumption 4.6 (with certain \mathcal{W}). Suppose f_θ satisfies Assumption K.1. Then there exist at least $(n^n - n!)$ distinct $w \in \mathcal{W}$ that are not global-min-reachable.

Proposition K.2. (*formal version of Prop. 2*): Consider the RpGAN problem $\min_{w \in \mathbb{R}^K} \varphi_R(w)$, where $\varphi_R(w) = \sup_{\theta} \frac{1}{n} \sum_{i=1}^n [h(f_\theta(x_i)) - f_\theta(G_w(z_i))]$. Suppose h satisfies the same assumptions of Theorem 2. Suppose G_w satisfies Assumption K.2 and Assumption 4.6 (with certain \mathcal{W}). Suppose f_θ satisfies Assumption K.1. Then any $w \in \mathcal{W}$ is global-min-reachable for $\varphi_R(w)$.

We have presented two generic results that relies on a few properties of the neural-nets. These properties can be satisfied by certain neural-nets, as discussed next. Our results largely rely on recent advanced in neural-net optimization theory.

K.1 Sufficient Conditions for the Assumptions

In this part, we present a set of conditions on neural nets that ensure the assumptions to hold. We will discuss more conditions in the next subsection.

Assumption K.4. (*mildly wide*): The last hidden layer has at least \bar{n} neurons, where \bar{n} is the number of input vectors.

The assumption of width is common in recent theoretical works in neural net optimization (e.g. [50, 73, 2]). For the generator network, we set $\bar{n} = n$; for the discriminator network, we set $\bar{n} = 2n$.

Assumption K.5. (*smooth enough activation*) *The activation function σ is an analytic function, and the k -th order derivatives $\sigma^{(k)}(0)$ are non-zero, for $k = 0, 1, 2, \dots, \bar{n}$, where \bar{n} is the number of input vectors.*

The assumption of the neuron activation is satisfied by sigmoid, tanh, SoftPlus, swish, etc.

For the generator network, consider a fully neural network $G_w(z) = W_H \sigma(W_{H-1} \dots W_2 \sigma(W_1 z))$ that maps $z \in \mathbb{R}^{d_z}$ to $G_w(z) \in \mathbb{R}^d$. Define $T_k(z) = \sigma(W_{k-1} \dots W_2 \sigma(W_1 z)) \in \mathbb{R}^{d_k}$ where d_k is the number of neurons in the k -th hidden layer. Then we can write $G_w(z) = W_H T_H(z)$, where $W_H \in \mathbb{R}^{d \times d_H}$. Let $Z = (z_1, \dots, z_n)$ and let $T_k(Z) = (T_k(z_1), \dots, T_k(z_n)) \in \mathbb{R}^{d_k \times n}$, $k = 1, 2, \dots, H$. Define $\mathcal{W} = \{w = (W_1, \dots, W_H) : T_H(Z) \text{ is full rank}\}$.

We will prove that under these two assumptions on the neural nets, the landscape of RpGAN is better than that of SepGAN.

Proposition K.3. *Suppose h_1, h_2, h satisfy assumptions in Theorem 1 and Theorem 2. Suppose G_w, f_θ satisfies Assump. K.5 and K.4 ($\bar{n} = n$ for G_w , and $\bar{n} = 2n$ for f_θ). Then there exist at least $(n^n - n!)$ distinct $w \in \mathcal{W}$ that are not GMR for $\varphi_{\text{Sep}}(w)$. In contrast, any $w \in \mathcal{W}$ is global-min-reachable for $\varphi_{\text{R}}(w)$.*

This proposition is the corollary of Prop. K.1 and Prop. K.2; we only need to verify the assumptions in the two propositions. The following series of claims provide such verification.

Claim K.1. *Suppose Assumptions K.4 and K.5 hold for the generator net G_w with distinct input z_1, \dots, z_n . Then $\mathcal{W} = \{(W_1, \dots, W_H) : T_H(Z) \text{ is full rank}\}$ is a dense set in \mathbb{R}^K . In addition, Assumption K.2 holds.*

This full-rank condition was used in a few works of neural-net landscape analysis (e.g. [72]). In GAN area, [7] studied invertible generator nets G_w where the weights are restricted to a subset of \mathbb{R}^K to avoid singularities. As the set \mathcal{W} is dense, intuitively the iterates will stay in this set for most of the time. However, rigorously proving that the iterates stay in this set is not easy, and is one of the major challenges of current neural-network analysis. For instance, [38]) shows that for very wide neural networks with proper initialization along the training trajectory of gradient descent the neural-tangent kernel (a matrix related to $T_H(Z)$) is full rank. A similar analysis can prove that the matrix $T_H(Z)$ stays full rank during training under similar conditions. We do not attempt to develop the more complicated convergence analysis for general neural-nets here and leave it to future work.

Claim K.2. *Suppose Assumptions K.4 and K.5 hold for the generator net G_w with distinct input z_1, \dots, z_n . Then it satisfies Assumption 4.6 with \mathcal{W} defined in Claim K.1.*

Assumption K.1 can be shown to hold under a similar condition to that in Claim K.1.

Claim K.3. *Consider a fully connected neural network $f_\theta(z) = \theta_H \sigma(\theta_{H-1} \dots \theta_2 \sigma(\theta_1 z))$ that maps $u \in \mathbb{R}^d$ to $f_\theta(u) \in \mathbb{R}$ and suppose Assumptions K.4 and K.5 hold. Then Assumption K.1 holds.*

The proofs of the claims are given in Appendix K.5.

With these claims, we can immediately prove Prop. K.3.

Proof of Prop. K.3: According to Claim K.2, K.1, K.3, the assumptions of Prop. K.3 imply the assumptions of Prop. K.1 and Prop. K.2. Therefore, the conclusions of Prop. K.1 and Prop. K.2 hold. Since the conclusion of Prop. K.3 is the combination of the the conclusions of Prop. K.1 and Prop. K.2, it also holds. \square

K.2 Other Sufficient Conditions

Assumption K.3 (path-keeping property) is the key assumption. Various results in neural-net theory can ensure this assumption (or its variant) holds, and we have utilized one of the simplest such results in the last subsection. We recommend to check [80] which describes a bigger picture about various landscape results. In this subsection, we briefly discuss other possible results applicable to GAN.

We start with a strong conjecture about neural net landscape, which only requires a wide final hidden layer but no condition on the depth and activation.

Conjecture K.1. *Suppose g_θ is a fully connected neural net with any depth and any continuous activation, and it satisfies Assumption K.4 (i.e. a mildly wide final hidden layer). Assume $\ell(y, \hat{y})$ is convex in \hat{y} , then the empirical loss function of a supervised learning problem $\sum_{i=1}^n \ell(y_i, g_\theta(x_i))$ is global-min-reachable for any point.*

We then describe a related conjecture for GAN, which is easy to prove if Conjecture K.1 holds.

Conjecture 1 (informal): Suppose G_w is a fully connected net satisfying Assump. K.4 (i.e. a mildly wide final hidden layer). Suppose G_w and f_θ are expressive enough (i.e. Assump. K.2 and Assump. K.1 hold). Then the RpGAN loss has a benign landscape, in the sense that any point is GMR for $\varphi_R(w)$. In contrast, the SepGAN loss does not have this property.

Unfortunately, we are not aware of any existing work that has proved Conjecture K.1, thus we are not able to prove Conjecture 1 above for now. Venturi et al. [84] proved a special case of Conjecture K.1 for $L = 1$ (one hidden layer), and other works such as Li et al. [50] prove a weaker version of Conjecture K.1; see [80] for other related results. The precise version of Conjecture K.1 seems non-trivial to prove.

We list two results on GAN that can be derived from weaker versions of Conjecture K.1; both results apply to the whole space instead of the dense subset \mathcal{W} .

Result 1 (1-hidden-layer): Suppose G_w is 1-hidden-layer network with any continuous activation. Suppose it satisfies Assump. K.4 (i.e. a mildly wide final hidden layer). Suppose G_w and f_θ are expressive enough (i.e. Assump. K.2 and Assump. K.1 hold). Then the RpGAN loss satisfies GMR for any point. This result is based on Venturi et al. [84].

Result 2: Suppose G_w is a fully connected network with any continuous activation and any number of layers. Suppose it satisfies Assump. K.4 (i.e. a mildly wide final hidden layer). Suppose G_w and f_θ are expressive enough (i.e. Assump. K.2 and K.1 hold). Then the RpGAN loss has no sub-optimal set-wise local minima (see [50, Def. 1] for the definition). This result is based on Li et al. [50].

Due to space constraint, we do not present the proofs of the above two results (combining them with GANs is somewhat cumbersome). The high-level proof framework is similar to that of Prop. K.3.

K.3 Proofs of Propositions for Parameter Space

Proof of Proposition K.1. The basic idea is to build a relation between the points in the parameter space to the points in the function space.

Denote $\mathcal{L}_{\text{sep}}(w; \theta) = \frac{1}{2n} \sum_{i=1}^n [h_1(f_\theta(x_i)) + h_2(-f_\theta(G_w(z_i)))]$, then $\varphi_{\text{sep}}(w) = \sup_\theta \mathcal{L}_{\text{sep}}(w; \theta)$. Denote $L_{\text{sep}}(Y; f) = \frac{1}{2n} \sum_{i=1}^n [h_1(f(x_i)) + h_2(-f(y_i))]$, and $\phi(Y, X) = \sup_f L_{\text{sep}}(Y; f)$. Note that in the definition of the two functions above, the discriminator is hidden in the sup operators, thus we have freedom to pick the discriminator values (unlike the generator space which we have to check all w in the inverse of Y).

Our goal is to analyze the landscape of $\varphi_{\text{sep}}(w)$, based on the previously proved result on the landscape of $\phi(Y, X)$. We first show that the image of $\varphi_{\text{sep}}(\hat{w})$ is the same as that of $\phi_{\text{sep}}(\hat{Y}, X)$.

Define $G^{-1}(Y) \triangleq \{w : G_w(z_i) = y_i, i = 1, \dots, n\}$. We first prove that

$$\phi_{\text{sep}}(\hat{Y}, X) = \varphi_{\text{sep}}(\hat{w}), \forall \hat{w} \in G^{-1}(\hat{Y}). \quad (33)$$

Suppose $\phi_{\text{sep}}(\hat{Y}, X) = \alpha$. This implies that $L_{\text{sep}}(\hat{Y}; f) \leq \alpha$ for any f ; in addition, for any $\epsilon > 0$ there exists $\hat{f} \in C(\mathbb{R}^d)$ such that

$$L_{\text{sep}}(\hat{Y}; \hat{f}) \geq \alpha - \epsilon. \quad (34)$$

According to Assumption K.1, there exists θ^* such that $f_{\theta^*}(x_i) = \hat{f}(x_i), \forall i$, and $f_{\theta^*}(u) = \hat{f}(u), \forall u \in \{y_1, \dots, y_n\} \setminus \{x_1, \dots, x_n\}$. In other words, there exists θ^* such that

$$f_{\theta^*}(x_i) = \hat{f}(x_i), f_{\theta^*}(y_i) = \hat{f}(y_i), \forall i. \quad (35)$$

Then we have

$$\begin{aligned}\mathcal{L}_{\text{sep}}(\hat{w}; \theta^*(\epsilon)) &= \frac{1}{2n} \sum_{i=1}^n [h_1(f_{\theta^*}(x_i)) + h_2(-f_{\theta^*}(G_{\hat{w}}(z_i)))] \stackrel{(i)}{=} \sum_{i=1}^n [h_1(f_{\theta^*}(x_i)) + h_2(-f_{\theta^*}(\hat{y}_j))] \\ &\stackrel{(ii)}{=} \frac{1}{2n} \sum_{i=1}^n [h_1(\hat{f}(x_i)) + h_2(-\hat{f}(\hat{y}_i))] = L_{\text{sep}}(\hat{Y}; \hat{f}) \stackrel{(iii)}{\geq} \alpha - \epsilon.\end{aligned}$$

In the above chain, (i) is due to the assumption $\hat{w} \in G^{-1}(\hat{Y})$ (which implies $G_{\hat{w}}(z_j) = \hat{y}_j$), (ii) is due to the choice of θ^* . (iii) is due to (34).

Therefore, we have $\varphi_{\text{sep}}(\hat{w}) = \sup_{\theta} \mathcal{L}_{\text{sep}}(\hat{w}; \theta) \geq \mathcal{L}_{\text{sep}}(\hat{w}; \theta^*(\epsilon)) \geq \alpha - \epsilon$. Since this holds for any ϵ , we have $\varphi_{\text{sep}}(\hat{w}) \geq \alpha$. Similarly, from $\mathcal{L}_{\text{sep}}(\hat{w}; \theta) \leq \alpha$ we can obtain $\varphi_{\text{sep}}(\hat{w}) \leq \alpha$. Therefore $\varphi_{\text{sep}}(\hat{w}) = \alpha = \phi_{\text{sep}}(\hat{Y}, X)$. This finishes the proof of (33).

Define

$$Q(X) \triangleq \{Y = (y_1, \dots, y_n) \mid y_i \in \{x_1, \dots, x_n\}, i \in \{1, 2, \dots, n\}; y_i = y_j \text{ for some } i \neq j\}.$$

Any $Y \in Q(X)$ is a mode-collapsed pattern. According to Theorem 1, any $Y \in Q(X)$ is a strict local minimum of $\phi_{\text{sep}}(Y, X)$, and thus Y is not GMR. Therefore $\hat{w} \in G^{-1}(Y)$ where $Y \in Q(X)$ is not GMR; this is because a non-decreasing path in the parameter space will be mapped to a non-decreasing path in the function space, causing contradiction. Finally, according to Assumption K.2, for any Y there exists at least one pre-image $w \in G^{-1}(Y) \cap \mathcal{W}$. There are $(n^n - n!)$ elements in $Q(X)$, thus there are at least $(n^n - n!)$ points in \mathcal{W} that are not global-min-reachable. \square

Proof of Proposition K.2. Similar to Eq. (33), we have $\varphi_{\text{R}}(w) = \phi_{\text{R}}(Y, X)$ for any $w \in G^{-1}(Y)$. We need to prove that there is a non-decreasing path from any $w_0 \in \mathcal{W}$ to w^* , where w^* is a certain global minimum. Let $Y_0 = G_{w_0}(z_1, \dots, z_n)$. According to Thm. 2, there is a continuous path $Y(t)$ from Y_0 to Y^* along which the loss value $\phi_{\text{R}}(Y(t), X)$ is non-increasing. According to Assump. 4.6, there is a continuous path $w(t)$ such that $w(0) = \hat{w}$, $Y(t) = G_{w(t)}(Z)$, $t \in [0, 1]$. Along this path, the value $\varphi_{\text{R}}(w(t)) = \phi_{\text{R}}(Y(t), X)$ is non-increasing, and at the end the function value $\varphi_{\text{R}}(w(1)) = \phi_{\text{R}}(Y^*, X)$ is the minimal value of $\varphi_{\text{R}}(w)$. Thus the existence of such a path is proved. \square

K.4 A technical lemma

We present a technical lemma, that slightly generalizes [50, Proposition 1].

Assumption K.6. $v_1, v_2, \dots, v_m \in \mathbb{R}^d$ are distinct, i.e., $v_i \neq v_j$ for any $i \neq j$.

Lemma 2. Define $T_H(V) = (\sigma(W_{H-1} \dots W_2 \sigma(W_1 v_i)))_{i=1}^m \in \mathbb{R}^{d_H \times m}$. Suppose Assumptions K.4, K.5 and K.6 hold. Then the set $\Omega = \{(W_1, \dots, W_{H-1}) : \text{rank}(T_H(V)) < m\}$ has zero measure.

This claim is slightly different from [50, Proposition 1], which requires the input vectors to have one distinct dimension (i.e., there exists j such that v_{1j}, \dots, v_{mj} are distinct); here we only require the input vectors to be distinct. It is not hard to link “distinct vectors” to “vectors with one distinct dimension” by a variable transformation.

Claim K.4. Suppose $v_1, \dots, v_m \in \mathbb{R}^d$ are distinct. Then for generic matrix $W \in \mathbb{R}^{d \times d}$, for the vectors $\bar{v}_i = W v_i \in \mathbb{R}^d$, $i = 1, \dots, m$, there exists j such that $\bar{v}_{1j}, \dots, \bar{v}_{mj}$ are distinct.

Proof. Define the set $\Omega_0 = \{u \mid u \in \mathbb{R}^{1 \times d}, \exists i \neq j \text{ s.t. } u^T v_i = u^T v_j\}$. This is the union of $d(d-1)$ hyperplanes $\Omega_{ij} \triangleq \{u \mid u \in \mathbb{R}^{1 \times d}, u^T v_i = u^T v_j\}$. Each hyperplane Ω_{ij} is a zero-measure set, thus the union of them Ω_0 is also a zero-measure set. Let u be the first row of W , then u is generic vector and thus not in Ω_0 , which implies $\bar{v}_{11}, \dots, \bar{v}_{m1}$ are distinct. \square

Proof of Lemma 2: Pick a generic matrix $A \in \mathbb{R}^{d_v \times d_v}$, then $\bar{v}_i = A v_i \in \mathbb{R}^{d_v \times 1}$ has one distinct dimension, i.e., there exists j such that $\bar{v}_{1j}, \dots, \bar{v}_{mj}$ are distinct. In addition, we can assume A is full rank (since it is generic). Define

$$\bar{T}_H(\bar{V}) = (\sigma(W_{H-1} \dots W_2 \sigma(\bar{W}_1 \bar{v}_1)), \dots, \sigma(W_{H-1} \dots W_2 \sigma(\bar{W}_1 \bar{v}_m))) \in \mathbb{R}^{d_H \times m}.$$

According to [50, Prop. 1], the set $\bar{\Omega} = \{(\bar{W}_1, W_2, W_3, \dots, W_{H-1}) : \text{rank}(\bar{T}_H(\bar{V})) < m\}$ has zero measure. With the transformation $\eta_0(\bar{W}_1) = \bar{W}_1 A^{-1}$, we have $\sigma(W_{H-1} \dots W_2 \sigma(\bar{W}_1 \bar{v}_i)) =$

$\sigma(W_{H-1} \dots W_2 \sigma(W_1 v_i))$, $\forall i$ and thus $\bar{T}_H(\bar{V}) = T_H(V)$. Define $\eta(\bar{W}_1, W_2, \dots, W_m) = (\bar{W}_1 A^{-1}, W_2, \dots, W_m)$, then η is a homeomorphism between $\bar{\Omega}$ and Ω . Therefore the set $\Omega = \{(W_1, \dots, W_{H-1}) : \text{rank}(T_H(V)) < m\}$ has zero measure. \square

K.5 Proof of claims

Proof of Claim K.1: According to Lemma 2, \mathcal{W} is a dense subset of \mathbb{R}^J (in fact, Ω is defined for a general neural network, and \mathcal{W} is defined for the generator network, thus an instance of Ω). As a result, there exists (W_1, \dots, W_{H-1}) such that $T_H(Z)$ has rank at least n . Thus for any $y_1, y_2, \dots, y_n \in \mathbb{R}^d$, there exists W_H such that $W_H T_H(Z) = (y_1, \dots, y_n)$. \square

Proof of Claim K.2: For any continuous path $Y(t), t \in [0, 1]$ in the space $\mathbb{R}^{d \times n}$, any $w_0 \in G^{-1}(Y(0))$ and any $\epsilon > 0$, our goal is to show that there exists a continuous path $w(t), t \in [0, 1]$ such that $w(0) = w_0$ and $Y(t) = G_{w(t)}(Z), t \in [0, 1]$.

Due to the assumption of $w_0 \in \mathcal{W}$, we know that w_0 corresponds to a rank- n post-activation matrix $T_H(Z)$. Suppose $w_0 = (W_1, \dots, W_H)$ and $T_H(Z) = (T_H(z_1), \dots, T_H(z_n)) \in \mathbb{R}^{d_H \times n}$ has rank n . Since $T_H(Z)$ is full rank, for any path from $Y(0)$ to $Y(1)$, we can continuously change W_H such that the output of $G_w(Z)$ changes from $Y(0)$ to $Y(1)$. Thus there exists a continuous path $w(t), t \in [0, 1]$ such that $w(0) = w_0$ and $Y(t) = G_{w(t)}(Z), t \in [0, 1]$. \square

Proof of Claim K.3: This is a direct application of Lemma 2. Different from Claim K.2, here we apply Lemma 2 to the discriminator network. \square

L Discussion of Wasserstein GAN

W-GAN is a popular formulation of GAN, so a natural question is whether we can prove a similar landscape result for W-GAN. Consider W-GAN formulation (empirical version) $\min_Y \phi_W(Y, X)$, where

$$\phi_W(Y, X) = \max_{|f|_L \leq 1} \frac{1}{n} \sum_{i=1}^n [f(x_i) - f(y_i)].$$

For simplicity we consider the same number of generated samples and true samples. It can be viewed as a special case of RpGAN where $h(t) = -t$; it can also be viewed as a special case of SepGAN where $h_1(t) = h_2(t) = -t$.

However, the major complication is the Lipschitz constraint. It makes the computation of the function values much harder. For the case of $n = 2$, the function value of $\phi_W(Y, X)$ is provided in the following claim.

Claim L.1. *Suppose $n = 2$. Denote $a_1 = x_1, a_2 = x_2, a_3 = y_1, a_4 = y_2$. The value of $\phi_W(Y, X)$ is*

$$\begin{aligned} & \max_{u_1, u_2, u_3, u_4 \in \mathbb{R}} u_1 + u_2 - u_3 - u_4, \\ & \text{s.t. } |u_i - u_j| \leq \|a_i - a_j\|, \forall i, j \in \{1, 2, 3, 4\}. \end{aligned}$$

This claim is not hard to prove, and we skip the proof here.

This claim indicates that computing $\phi_W(Y, X)$ is equivalent to solving a linear program (LP). Solving LP itself is computationally feasible, but our landscape analysis requires to infer about the global landscape of $\phi_W(Y, X)$ as a function of Y . In classical optimization, it is possible to state that the optimal value of an LP is a convex function of a certain parameter (e.g. the coefficient of the objective). But in our LP y_i 's appear in multiple positions of the LP, and we are not aware of an existing result that can be readily applied.

Similar to Kantorovich-Rubinstein Duality, we can write down the dual problem of the LP where the objective is linear combination of $\|a_i - a_j\|$. However, it is still not clear what to say about the global landscape, due to the lack of closed-form solutions.

Finally, we remark that although W-GAN has a strong theoretical appeal, it did not replace JS-GAN or simple variants of JS-GAN in recent GAN models. For instance, SN-GAN [67] and BigGAN [18] use hinge-GAN.

(a) Generator	(b) Discriminator
$z \in \mathbb{R}^{128} \sim \mathcal{N}(0, I)$	image $x \in [-1, 1]^{H \times W \times 3}$
$128 \rightarrow h \times w \times 512/c$, dense, linear	3×3 , stride 1 conv, $64/c$
4×4 , stride 2 deconv, $256/c$, BN, ReLU	4×4 , stride 2 conv, $128/c$ 3×3 , stride 1 conv, $128/c$
4×4 , stride 2 deconv, $128/c$, BN, ReLU	4×4 , stride 2 conv, $256/c$ 3×3 , stride 1 conv, $256/c$
4×4 , stride 2 deconv, $64/c$, BN, ReLU	4×4 , stride 2 conv, $512/c$ 3×3 , stride 1 conv, $512/c$
3×3 , stride 1 conv, 3, Tanh	$h \times w \times 512/c \rightarrow s$, linear

Table 7: CNN models for CIFAR-10 and STL-10 used in our experiments on image Generation. $h = w = 4$, $H = W = 32$ for CIFAR-10. $h = w = 6$, $H = W = 48$ for STL-10. $c=1, 2$ and 4 for the regular, 1/2 and 1/4 channel structures respectively. All layers of D use LReLU-0.1 (except the final dense “linear” layer).

(a) Generator	(b) Discriminator
$z \in \mathbb{R}^{128} \sim \mathcal{N}(0, I)$	image $x \in [-1, 1]^{32 \times 32 \times 3}$
dense, $4 \times 4 \times 256/c$	ResBlock down $128/c$
ResBlock up $256/c$	ResBlock down $128/c$
ResBlock up $256/c$	ResBlock down $128/c$
ResBlock up $256/c$	ResBlock down $128/c$
BN, ReLU, 3×3 conv, 3 Tanh	LReLU 0.1
	Global sum pooling
	dense $\rightarrow 1$

Table 9: Resnet architecture for CIFAR-10. $c=1, 2$ and 4 for the regular, 1/2 and 1/4 channel structures respectively.

(a) Generator	(b) Discriminator
$z \in \mathbb{R}^{128} \sim \mathcal{N}(0, I)$	image $x \in [-1, 1]^{32 \times 32 \times 3}$
dense, $4 \times 4 \times 128$	BRes down (64, 32, 64)
BRes up (128, 64, 128)	BRes down (64, 32, 64)
BRes up (128, 64, 128)	BRes down (64, 32, 64)
BRes up (128, 64, 128)	BRes down (64, 32, 64)
BN, ReLU, 3×3 conv, 3 Tanh	LReLU 0.1
	Global sum pooling
	dense $\rightarrow 1$

Table 11: BottleNeck Resnet models for CIFAR-10. BRes refers to BottleNeck ResBlock. BRes (a, b, c) refers to the Bottleneck resblock with (input, hidden and output) being (a, b, c).

RS-GAN generator learning rate			
		CIFAR-10	STL-10
CNN	No normalization	2e-4	5e-4
	Regular + SN	5e-4	5e-4
	channel/2 + SN	5e-4	5e-4
	channel/4 + SN	2e-4	5e-4
ResNet	Regular+SN	1.5e-3	1e-3
	channel/2 + SN	1.5e-3	1e-3
	channel/4 + SN	1e-3	5e-4
	BottleNeck	1e-3	1e-3

Table 13: Learning rate for RS-GAN in each setting. Hyper-parameters used for WGAN-GP

(a) Generator	(b) Discriminator
$z \in \mathbb{R}^{128} \sim \mathcal{N}(0, I)$	$x \in [-1, 1]^{256 \times 256 \times 3}$
reshape $\rightarrow 128 \times 1 \times 1$	4×4 , stride 2 conv, 32,
4×4 , stride 1 deconv, BN, 1024	4×4 , stride 2 conv, 64
4×4 , stride 2 deconv, BN, 512	4×4 , stride 2 conv, 128
4×4 , stride 2 deconv, BN, 256	4×4 , stride 2 conv, 256
4×4 , stride 2 deconv, BN, 128	4×4 , stride 2 conv, 512
4×4 , stride 2 deconv, BN, 64	4×4 , stride 2 conv, 1024
4×4 , stride 2 deconv, BN, 32	dense $\rightarrow 1$
4×4 , stride 2 deconv, 3, Tanh	

Table 8: CNN model architecture for size 256 LSUN used in our experiments on high resolution image generation. All layers of G use ReLU (except one layer with Tanh); all layers of D use LReLU-0.1.

(a) Generator	(b) Discriminator
$z \in \mathbb{R}^{128} \sim \mathcal{N}(0, I)$	image $x \in [-1, 1]^{48 \times 48 \times 3}$
dense, $6 \times 6 \times 512/c$	ResBlock down $64/c$
ResBlock up $256/c$	ResBlock down $128/c$
ResBlock up $128/c$	ResBlock down $256/c$
ResBlock up $64/c$	ResBlock down $512/c$
BN, ReLU, 3×3 conv, 3 Tanh	ResBlock down $1024/c$
	LReLU 0.1
	Global sum pooling
	dense $\rightarrow 1$

Table 10: Resnet architecture for STL-10. $c=1, 2$ and 4 for the regular, 1/2 and 1/4 channel structures respectively.

(a) Generator	(b) Discriminator
$z \in \mathbb{R}^{128} \sim \mathcal{N}(0, I)$	image $x \in [-1, 1]^{48 \times 48 \times 3}$
dense, $6 \times 6 \times 256$	BRes down (3, 16, 32)
BRes up (256, 64, 128)	BRes down (32, 16, 64)
BRes up (128, 32, 64)	BRes down (64, 32, 128)
BRes up (64, 16, 32)	BRes down (128, 64, 256)
BN, ReLU, 3×3 conv, 3 Tanh	BRes down (256, 128, 512)
	LReLU 0.1
	Global sum pooling
	dense $\rightarrow 1$

Table 12: BottleNeck Resnet models for STL-10.

WGAN-GP Hyper-parameters	
generator learning rate	1e-4
discriminator learning rate	1e-4
β_1	0.5
β_2	0.9
Gradient penalty λ	10
# D iterations per G iteration	5

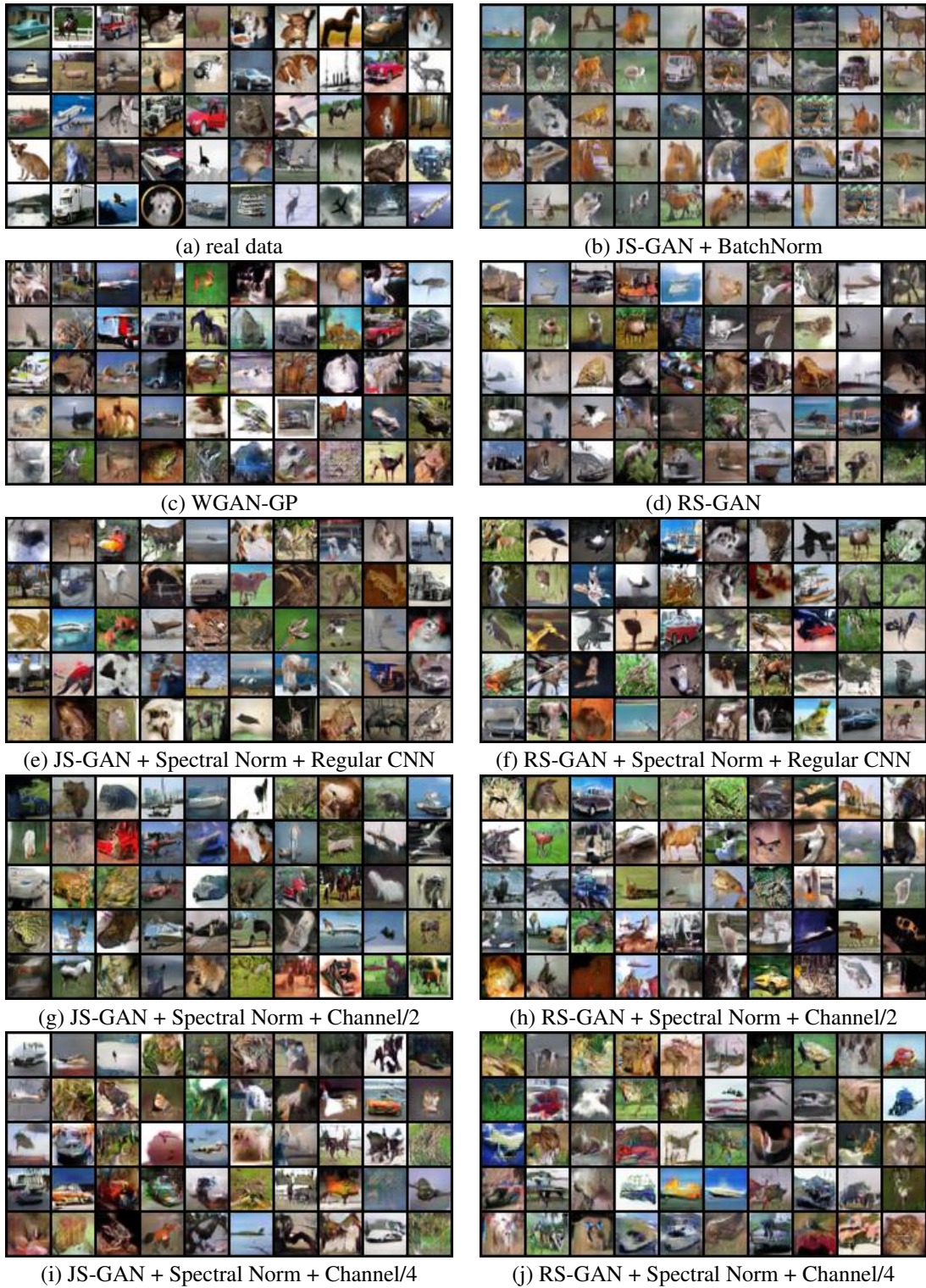


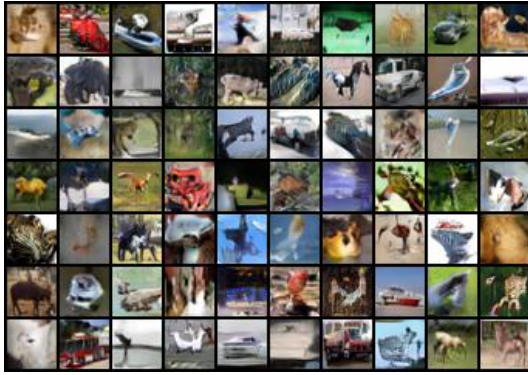
Figure 16: Generated CIFAR-10 samples with CNN.



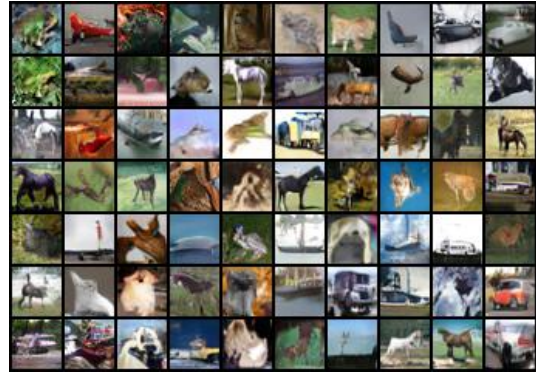
(a) JS-GAN + Spectral Norm + Regular ResNet



(b) RS-GAN + Spectral Norm + Regular ResNet



(c) JS-GAN + Spectral Norm + Channel/2



(d) RS-GAN + Spectral Norm + Channel/2



(e) JS-GAN + Spectral Norm + Channel/4



(f) RS-GAN + Spectral Norm + Channel/4



(g) JS-GAN + Spectral Norm + BottleNeck



(h) RS-GAN + Spectral Norm + BottleNeck

Figure 17: Generated CIFAR-10 samples on ResNet.

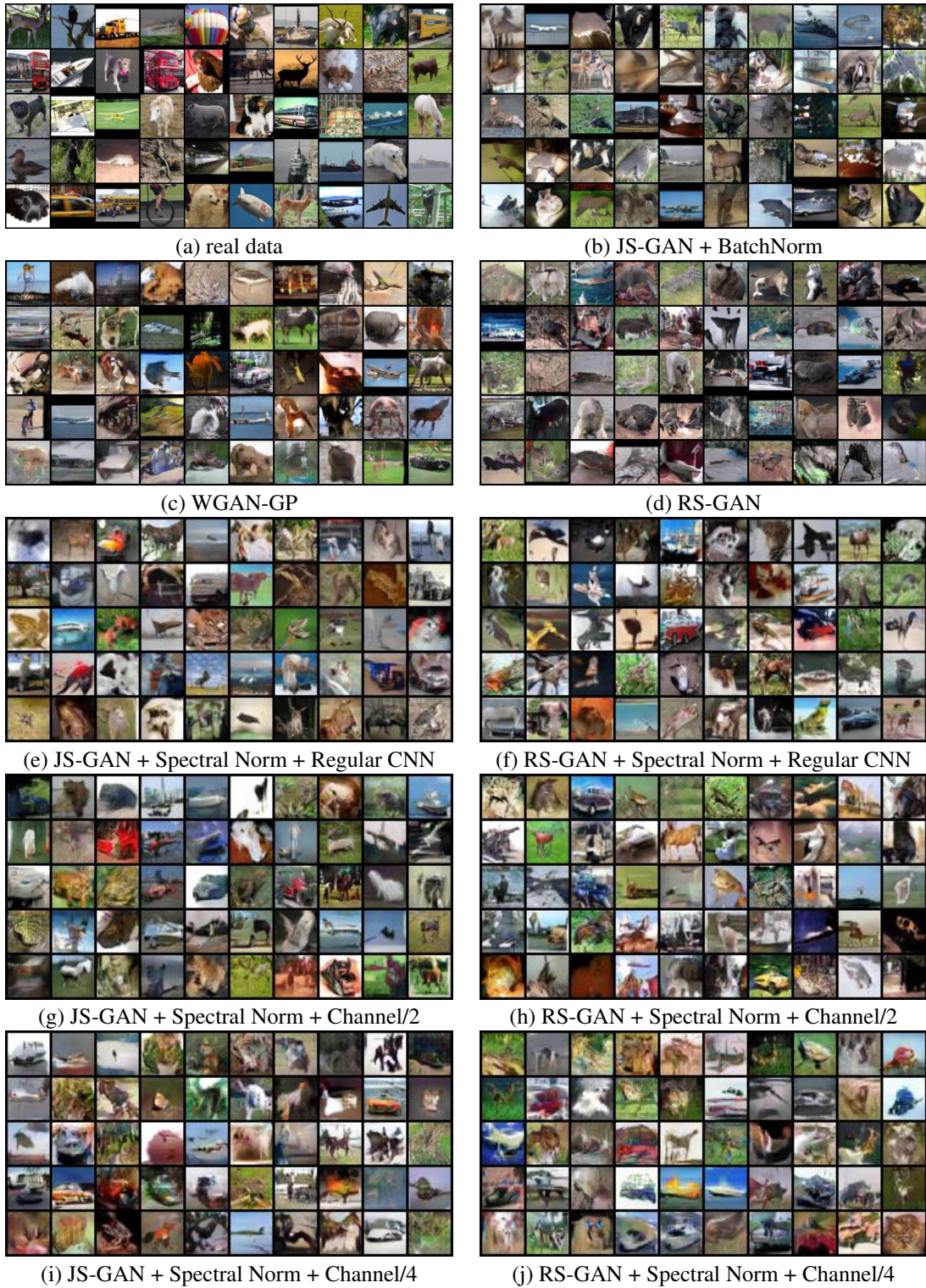


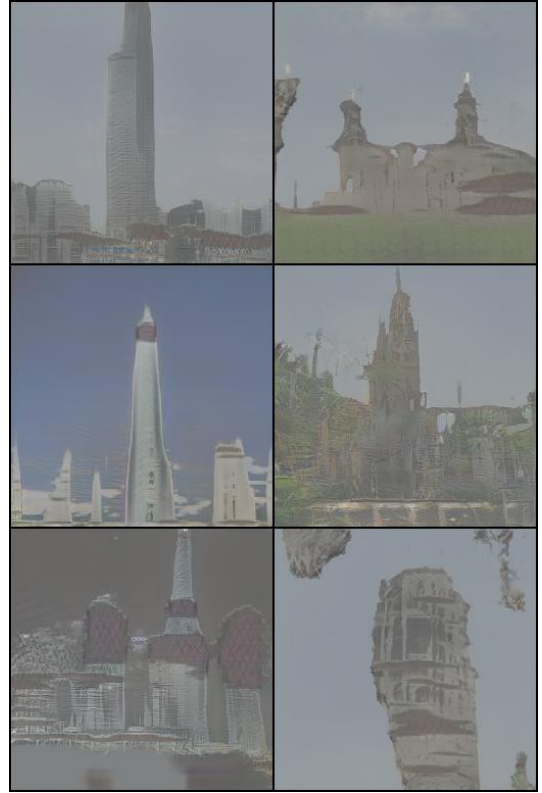
Figure 18: Generated STL-10 samples with CNN.



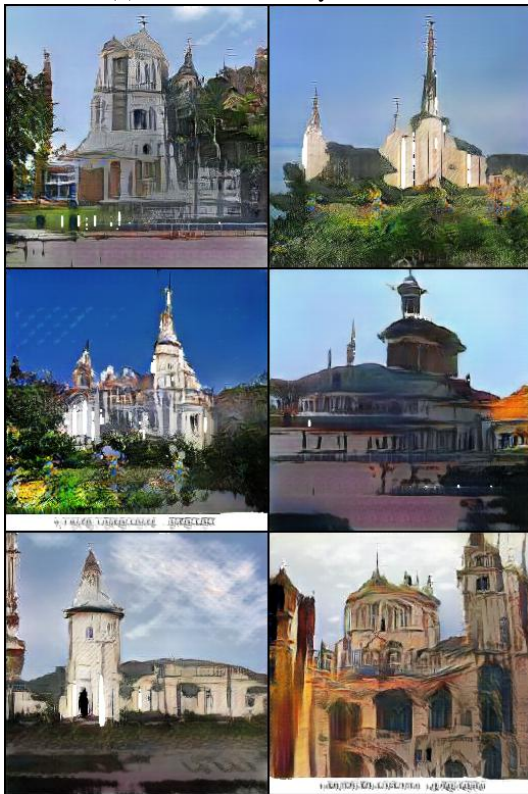
Figure 19: Generated STL-10 samples with ResNet.



(a) LSUN Church by JS-GAN



(b) LSUN Tower by JS-GAN



(c) LSUN Church by RS-GAN



(d) LSUN Tower by RS-GAN

Figure 20: Generated 256×256 Church and Tower Image by JS-GAN and RS-GAN.